Towards optimized membranes for aqueous organic redox flow batteries: Correlation between membrane properties and cell performance

Misgina Tilahun Tsehaye, Gaël Mourouga, Thomas Schmidt, Juergen Schumacher, Svetlozar Velizarov, Bart van der Bruggen, Fannie Alloin, Cristina Iojoiu

Towards Optimised Membranes for Aqueous Organic Redox Flow Batteries: Correlation Between Membrane Properties and Cell Performance

Misgina Tilahun Tsehaye[a,b,1,*], Gaël Mourouga[c,1,*], Thomas J. Schmidt[d,e], Juergen O. Schumacher[c], Svetlozar Velizarov[f], Bart Van der Bruggen[g], Fannie Alloin[b], Cristina Iojoiu[b]

[a]Separation Conversion Technology, Flemish Institute for Technological Research (VITO), Boeretang 200, 2400 Mol, Belgium

[b]Univ. Grenoble Alpes, Univ. Savoie Mont Blanc, CNRS, Grenoble INP, LEPMI, 38 000 Grenoble, France

[c]Institute of Computational Physics, ZHAW, Wildbachstr. 21, CH-8400 Winterthur, Switzerland

[d]Paul Scherrer Institut, Electrochemical Laboratory, Forschungsstrasse 111, CH-5232 Villigen PSI, Switzerland

[e]ETH Zurich, Laboratory for Physical Chemistry, CH-8092 Zurich, Switzerland

[f]LAQV-REQUIMTE, Department of Chemistry, NOVA School of Science and Technology, FCT NOVA, Universidade Nova de Lisboa, 2829-516,Caparica, Portugal

[g]Department of Chemical Engineering, KU Leuven, Celestijnenlaan 200F, B-3001 Leuven, Belgium

Corresponding authors:

Misgina Tilahun Tsehaye (misginabcen@gmail.com), Gaël Mourouga (gaelmourouga@protonmail.com)

[1]Both authors contributed equally to this work.

Abstract

Aqueous organic redox-flow batteries (AORFBs) are an emerging technological solution in the field of grid-scale energy storage, owing to their long lifetime, safety, chemical flexibility, potentially low costs and environmental friendliness. Membranes are a crucial component of the battery as they affect the ohmic resistance and the power density of the cells, as well as the depth-of-discharge and the lifetime and thus, crucially affect the levelised cost of storage of the battery. Herein, we provide a critical discussion of the state-of-the-art literature on membranes for AORFBs, including a summary on the theories used to model the transport of ions and active species through the membrane, as well as a compilation of experimental correlations between various membrane properties and cell performance. Adequate strategies to further improve the performance and lower the cost of AORFBs by employing and designing appropriate membranes are highlighted. Finally, the remaining challenges are summarised and perspectives on future research directions for developing appropriate and low-cost membranes for AORFBs are outlined.

Keywords: Aqueous organic redox flow battery, Ion exchange membranes, Capacity fade, Power density, Energy efficiency

1. Introduction

In the last decades, the energy sector has been increasingly challenged by a combination of increasing demand, climate change, and a shift away from fossil fuel-powered generation. Most low-carbon energy sources being deployed massively on electric grids around the world, such as solar and wind, produce intermittent electrical power based on time, spatial and climatic factors. Since the electric grid provides the cornerstone for economic progress in almost every industrialized country on the planet, this has lead to 1 to 2 per cent of Gross Domestic Product (GDP) growth loss due to blackouts, over-investment in backup electricity generators, and inefficient use of resources [1].

High-performance and cost-effective energy storage technologies are thus required for frequency regulation and peak-shaving applications to improve the grid's stability [2][3]. Among these technologies, batteries have recently seen a surge in popularity, owing to their flexibility of installation and lower capital costs required compared to larger centralized storage technologies (such as pumped hydro), thus allowing the transition from a centralized grid model to a network of smart, decentralized microgrids [4].

In this context, aqueous redox-flow batteries (RFBs) offer a number of significant advantages, including: long theoretical lifetime when compared to the more widespread lithium-ion technologies, leading to a lower potential levelized cost of storage (LCOS) at the industrial scale; decorrelation between energy and power sizing (the energy being proportional to the volume of the tanks, whereas the power is proportional to the nominal voltage and size of the stacks), leading to a greater flexibility in design to meet local grid requirements; and finally non-flammability due to the large volumes of water-based electrolytes, leading to a greater intrinsic reliability compared to technologies presenting the risk of thermal runaway (lithium-ion) or high flammability (hydrogen). Until recently, most electroactive materials used in aqueous RFBs were limited to transition metal redox couples, such as the all-vanadium RFB (VRFB), by far the most commonly used RFB system worldwide [5]–[7]. However, in both lithium-ion batteries and the all-vanadium flow battery, there is a concern about the environmental impact, sustainability and security of the supply chain of active materials, such as lithium, cobalt or vanadium.

For this reason, the idea of replacing transition metals with new organic aqueous soluble redox couples with fast electrochemical reaction kinetics, high tunability of molecular structure, low cost and no need for mining in the supply chain, has received increasing research interest in recent years [8]–[11].

Various organic materials-based chemistries have been developed, which can be classified into aqueous organic RFBs (AORFBs), non-aqueous ORFBs (NAORFBs) based on the nature of the solvent, and hybrid aqueous/non-aqueous ORFBs (HORFBs) based on the nature of the active materials [12]. Furthermore, depending on the pH of the electrolyte, AORFBs can be classified into acidic, basic and neutral. Compared to NAORFBs, the AORFBs provide relatively low-cost electrolyte, high ionic conductivity and fast kinetics [13], [14] and most importantly, greater industrial applications, lower sensitivity to oxygen, and milder conditions for the ion-exchange membranes, and therefore are the focus of this review. Various catholyte and anolyte active species such as benzoquinone or anthraquinone derivatives, viologens, 2,2,6,6-tetramethylpiperidine-1-oxyl (TEMPO) and alloxazine have been studied and reported in the literature. A number of molecular designing strategies of the organic redox-active materials have been employed in order to increase their solubility, cell voltage, stability, electrochemical reversibility, cyclability and performance at a high charge rate (C-rate) [11], [15], thus enhancing the power and energy density of AORFBs and making them a promising electrochemical energy storage technology [8], [9], [11], [16] with a rapidly rising number of patents being filed. Some all-organic and hybrid systems are nearing the point of commercialization, as illustrated in Figure 1 showing the chemistries of some European startups, namely Jena Batteries GmbH (Germany), KemiWatt (France) and Green Energy Storage (GES, Italy).

Membranes in AORFBs are used for the conduction of charge-carrying ions while preventing the cross-contamination of redox-active chemicals and, possibly, short-circuits. Compared to redox-active species, membranes remain a much less investigated component at the industrial scale. Ion-exchange membranes currently used in large-scale systems were originally developed for other applications, such as proton-exchange membrane fuel cells, desalination or acid recovery. AORFB chemistries, however, operate in a widely different range of conditions than the aforementioned applications, so it is not unlikely to see ion-exchange membranes with properties tailored to a specific chemistry outperform today’s commercially available membranes in the near future.

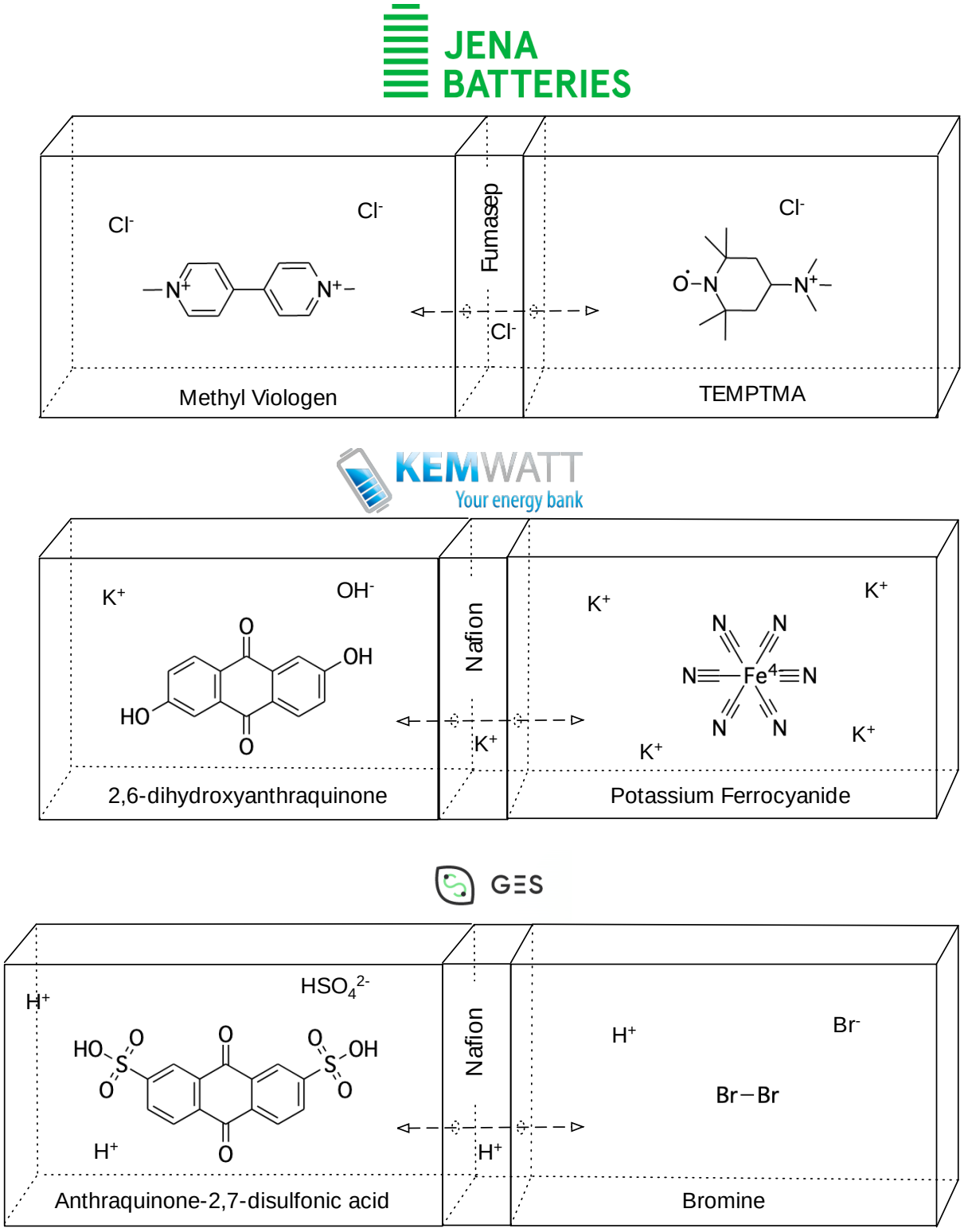

Figure 1: Scheme of some aqueous organic systems being developed at the industrial scale by European startups. From top to bottom: the TEMPTMA/Methyl Viologen all-organic system (neutral pH) developed by JenaBatteries GmbH (Germany), the anthraquinone/ferrocyanide hybrid system (basic pH) developed by KemiWatt (France) and the AQDS/Bromine system (acidic pH) developed by GreenEnergyStorage (Italy). Disclaimer: this figure is based on published data and may not be representative of these companies current generation of electrolytes.

Therefore, further research efforts on development of suitable, low-cost membranes are needed to improve the performance and lifetime of AORFBs and ultimately unlock the full potential of the battery. Herein, we critically discuss the key properties, state-of-the-art studies and future perspectives of membranes used in AORFBs (alkaline, neural and acidic) systems. Correlations between membrane properties and AORFBs cell performances have been analyzed. Moreover, remaining gaps and strategies for addressing them are provided.

This review paper is organized as follows: Section 2 discusses the key requirements and characteristics of membranes used in AORFBs. Mathematical modelling of ion, water and active species transport in membrane for AORFBs are discussed in section 3. Discussion on recent advances in membranes for neutral, alkaline and acidic AORFBs is provided in section 4. The remaining challenges are discussed, as well as strategies for overcoming them. Guidelines for selecting and designing appropriate membranes for AORFB systems are provided in section 5. Conclusions and perspectives for understanding membrane-cell relations and developing membranes for high-performance AORFB systems are provided.

2. Key characteristics of membranes for AORFBs

In the RFB, the membrane plays two critical and somewhat opposing roles: it must prevent the posolyte and negolyte from mixing over time, while allowing the charge carrier ions to pass in order to enable the electrochemical reaction. This implies a trade-off between a set of different properties: conducting properties (ionic conductivity, ion-exchange capacity), separating properties (permselectivity, permeability) and stability properties (electrochemical and mechanical stability). The following section aims at defining these properties and presenting different measurement methods to characterise ion-exchange membranes. Table 1 summarizes key properties of membranes commonly used in AORFBs.

2.1 Ion conduction properties

The conducting properties of an ion-exchange membrane relate to how well it can carry ions from one electrolyte to the other, ensuring electroneutrality during the electrochemical reaction and the transfer of electrons. Ion conduction is thought to occur primarily through water channels formed by phase separation between hydrophilic (ionic groups) and hydrophobic regions (polymer backbone) as illustrated in the graphical abstract of this publication.

2.1.1 Ion-exchange capacity

The ion-exchange capacity (IEC) relates to the amount of charged functional groups per unit volume of dry membrane, which are in interaction with water and mediate ion transport. The IEC of an ion-exchange membrane can be determined via titration [17]–[20] which measures the quantity of counter-ions released by the membrane in an external solution, by Nuclear Magnetic Resonance (NMR) [21], [22] or other methods such as Fourier-transform infrared spectroscopy (FTIR), energy-dispersive X-ray (EDX) and elemental analysis (EA) [23], [24] as shown in Figure 2. Overall, titration and Infrared spectroscopy present the highest uncertainties, and NMR should be favored when possible.

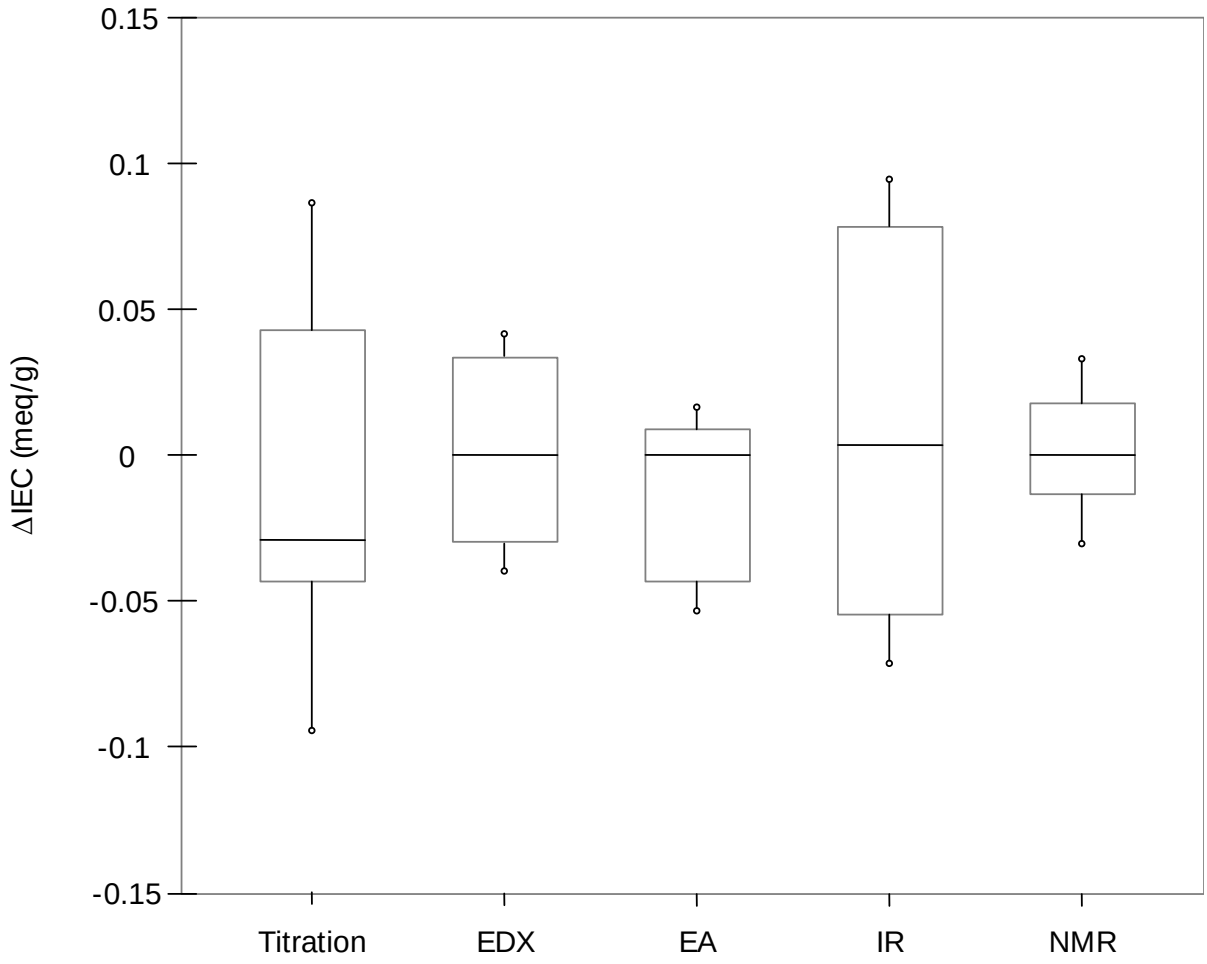

Figure 2: Uncertainties in the IEC values obtained from different experimental methods, reproduced from ref. [24]. The lower and upper edges of the boxes represent the 25th and 75th percentile values, respectively. The lower and upper whiskers represent the standard deviation, while the horizontal lines near the centre of each box represent the median value. Copyright Elsevier 2011.

2.1.2 Water uptake

The water uptake (WU) of a membrane is usually evaluated from the amounts of absorbed water and dry weight of the corresponding membrane samples:

$$WU = \frac{m_w - m_d}{m_d}, \quad (1)$$

where m_w represents the mass of the membrane measured after immersion of the membrane in DI water for an extended period of time [25] and m_d is the mass of the membrane after drying in a vacuum oven at high temperature for an extended period of time [25].

2.1.3 Ionic conductivity

The ionic conductivity, in its most formal definition, is a tensor σ relating the applied electric field E to the ionic current density j_i in the absence of concentration gradients [26]

$$j_i|_{\nabla c_i = 0} = \sigma_i \cdot E. \quad (2)$$

The transport of ions occurring predominantly in the through-plane direction, the conductivity is usually reported as a scalar σ, corresponding to the through-plane component of the conductivity tensor.

Several ways of measuring ionic conductivity of a membrane exist, which can be classified into DC (direct current) and AC (alternative current). DC methods can be further divided into "direct-contact methods", in which the ohmic resistance (with and without membrane) is measured in a two-electrode setup which sandwiches the membrane (no solution compartments), or "difference methods", in which a four- electrodes setup measures the ohmic resistance (with and without membrane) between two flowing salt solutions [27].

It should be noted that important discrepancies in the measurements can arise between different DC methods, e.g., the ionic conductivity of a Neosepta CMX cation-exchange membrane in 1 M NaCl was reported as 2 $mS.cm^{-1}$ by Pismenskaya et al. [28] but 7.3 $mS.cm^{-1}$ by Galama et al. [29] in the same conditions of temperature and pH, pointing to the lack of standards in measuring and reporting conductivity values [27]. This problem is further highlighted in Table 1 (where membrane area resistance is given instead of the ionic conductivity; two parameters are linked for a given commercial membrane which has a fixed thickness, see equation 3), where reported characteristics of the same commercially available membranes were compiled from different sources. Problems relative to DC methods, such as the formation of a diffusion boundary layer at the interface membrane/electrolyte, can be overcome by the use of AC methods, the most common of which is Electrochemical Impedance Spectroscopy (EIS) [30]–[32]. In EIS, a small alternating potential of known frequency ω and small amplitude u_0 is applied to the system. The amplitude i_0 and the phase difference ϕ of the electrical current that develops across the membrane are measured. The resulting impedance Z(ω) of the

membrane can be represented via a Nyquist plot, i.e., $-\mathrm{Im(Z)} = \mathrm{f(Re(Z))}$[33], where the membrane resistance $\mathrm{R_m}$ (Ω) is measured from the intersect with the *x* axis.

The membrane area resistance R_s $(\Omega.\,\mathrm{cm}^2)$ is then obtained by multiplying the measured membrane resistance $\mathrm{R_m}$ with its area *A* and is related to the membrane ionic conductivity σ ($\mathrm{S.cm^{-1}}$) according to the relationship

$$\sigma = \frac{\mathrm{l}}{\mathrm{R_s}}, \tag{3}$$

where *l* is the wet thickness of the membrane (cm) measured after immersion of the membrane in DI water for an extended period of time [25].

Basic membrane properties such as ion conductivity and water uptake are a function of a wide array of parameters, including external electrolyte nature and composition [27], temperature [34], microstructure [35], [36] nature of the membrane counter-ions [37] and have been shown to behave linearly as a function of IEC until a certain threshold, after which strongly non-linear increases occur [38], [39].

For copolymer membranes, it has been assumed that this corresponds to the percolation threshold, after which copolymers produce morphologically more open structure and basic membrane properties change drastically [22], [39].

2.2 Separation properties

2.2.1 Permselectivity

For an ion-exchange membrane, the term membrane permselectivity refers to its larger permeability to counterions than to co-ions. While porous membranes separate mainly based on size and steric effects [40], for ion-exchange membranes the Donnan charge-separation mechanism of counter-ions and co-ions is dominant [41]. The permselectivity (α) of an ion-exchange membrane can be linked to cell performance via the definition of transport number t_i [42], [43]:

$$\alpha = \frac{\mathrm{t_i^m} - \mathrm{t_i^s}}{1 - \mathrm{t_i^s}}, \tag{4}$$

where the subscript *i* corresponds to counter-ions and the superscripts s and m to solution and membrane, respectively. The ionic transport numbers represent the portion of the ionic current (in an electrolyte or a membrane) that is carried by ions, and are thus defined as the ratio between the ionic current and the total electric current

$$t_i = \frac{\mathrm{I_i}}{\mathrm{I}}, \tag{5}$$

where $I = F\sum_i z_i N_i$ is the total electric current in the system, where F refers to the Faraday constant, while $I_i = z_i F N_i$ is the current due to migration corresponding to a particular ion, where z_i is its charge and N_i is the molar flux of ion i through the membrane. Thus, a hypothetical perfectly permselective membrane with counter-ions transport number equal to 1 would exhibit a perfect separation of posolyte and anolyte. A common method to measure the permselectivity of ion-exchange membrane for flow battery applications is through membrane potential experiments [41], [43]–[47], a method which requires a simple experimental setup, i.e., two reservoirs of unlike concentrations of solute and two reference electrodes. The caveats are that the thermodynamic activities $a_{\pm}$ of the solute must be known, which is often not the case for AORFB chemistries, and that osmotic transfers must be negligible over the time-scale of the experiment [48].

Chronopotentiometry experiments [49]–[51] may also be used, but require a more advanced experimental setup, i.e., multiple flowing reservoirs (four [52] or six [53]), preferably thermostated and containing unlike electrolyte solutions and at least four electrodes (two references, one working and one counter-electrode) [49]. In these experiments, different values of current density *i* are applied to the membrane, and the voltage drop ΔV across the membrane is recorded. From the obtained chronopotentiometric curve, the transition time τ can be determined and transport numbers can be calculated from the Sand equation [54].

2.2.2 Solute permeability

In practice, membranes rarely exhibit a perfect permselectivity, leading to the crossover of active species and/or supporting electrolyte due to diffusion or migration through the membrane [55]. This crossover is usually studied *ex-situ* through static permeation experiments in diffusion cells (sometimes dynamic, involving currents [56]), where the concentration of active species in the reservoirs as a function of time is generally monitored via Ultraviolet (UV)-visible spectroscopy [57]–[59], most AORFB chemistries having identifiable UV spectra. Cyclic Voltammetry [60] can also be used for monitoring the concentration of electroactive material, with a lower resolution however than UV-visible spectroscopy. For monitoring the concentration of inert but conductive electrolytes (e.g., supporting electrolytes such as NaCl) conductivity probes [45], [61] may be used to monitor the concentration of materials in the reservoirs.

In these studies, the electrolyte is usually assumed to be infinitely dilute, so that an integration of Fick's law yields the following solution for the permeability coefficient [62]

$$P = -\frac{Vl}{2At}\ln\left(1 - 2\frac{C_r(t)}{C_0}\right), \quad (6)$$

where $C_r(t)$ is the concentration of permeating solute in the receiving phase, C_0 its initial concentration in the donating phase, *V* the volume of solution on both sides (assuming no osmosis), *t* the sampling time, *l* the membrane thickness and *A* its area.

2.2.3 Water permeability

An important hypothesis in Eq.(6) is that the volume of both reservoirs is constant. In the event where the osmotic pressure of solutions on both sides of the membrane is not equilibrated, water transfer may occur from the concentrated to the dilute side, water being transported along the direction of its decreasing chemical potential [63]. In that case, the volume on both sides of the membrane will not be a constant as a function of time, so that either a solute inert to UV-visible spectroscopy (e.g., NaCl) may be used to equilibrate the osmotic pressure [64], [65], osmosis and diffusion may be monitored through the same experimental setup [61], [66].

2.2.4. Compilation of membrane property from the literature

Table 1: Compilation of some commercial ion exchange membrane properties from the literature

Membrane	Company	*L (μm)*	IEC (meq.g^{-1})	WU (wt.%)	Rs (Ω.cm^2)	A (%)	PNaCl	Ref
Anion exchange membranes								
Selemion®AMV	AGC, Japan	109 ± 3[a]	2.02 ± 0.04[b]	19[c]			8.27 ± 0.08[d]	[61]
		104[d]	1.9	24	2.27			[57]
		107-124	1.78	17-20	3.15	87.3		[67]
Selemion®ASV	AGC, Japan	121 ± 5	2.02 ± 0.02	19			2.48 ± 0.21	[68]
		110	2.1	17.3	4.76			[57]
		120			3.7	97		[67]
Neosepta®AMX	Tokuyama Soda Co., Japan	133±1[a]	1.42±0.03[b]	16[c]			32.0±0.09[d]	[68]
		129-134	1.25	16-17.5	1.03-2.35[h]	90.7[i]		[67]
		138±2[j]	1.30±0.02	16.4±0.5[j]	2.65±0.04[h]	91±0.4[i]		[30]
Fumasep®FAS	Fumatech, Germany	30±1[a]	2.15±0.09[b]	12[c]			1.59±0.08d	[68]
		20-36	1.12-1.15	8-23.5	0.5-1.03[h]	89-96[i]		[67]
		28-31	1.6-2.0	15-30	0.80[g]	92-96		[69]
Cation exchange membranes								
Selemion®CMV	AGC, Japan	105±2[a]	1.89±0.09[b]	23[c]			14.5±0.06[d]	[68]
		101	2.01	20-30	2.29[h]	98.8[i]		[67]
Neosepta®CMX	Tokuyama Soda Co., Japan	170±4[a]	1.77±0.01[b]	22[c]			26.0±0.18[d]	[68]
		150	1.62-2	22-38	1.5-2.91[h]	94-99[i]		[67]
		181±2[j]	1.64±0.01	21.5±0.2[j]	3.43±0.16[h]	92.5±0.6[i]		[30]
Nafion®115	DuPont, USA	126±4[a]	0.92±0.01[b]	11[c]			42.4±0.27[d]	[68]

		127-161	0.96	17[k]		68[l]	47[d]	[45]
		127	0.95-1.01	38	2.11m			[70]
		139±8	0.9	11.02±0.02	1.5h	88[n]		[71]
Nafion®117	DuPont, USA	183-208	0.94	20[k]		69[l]	25[d]	[45]
		183	0.95-1.01	38	2.60[m]			[70]
		201±4	0.9	11.7±0.0%	1.8[h]	88[n]		[71]

Compilation of properties reported in the literature for different commercially available membranes, illustrating the variations in values reported due to different protocols or experimental techniques being used. The absence of index indicates values not measured in the publication (e.g., manufacturer values).

a:Wet thickness measured after experiments in contact with 4 M NaCl and water. b: IEC measured via titration with NaOH. c: Swelling degree measured gravimetrically after equilibration with 4M NaCl. d : Salt permeability measured via osmosis-diffusion experiment where NaCl concentration was monitored via a conductivity probe. e: Wet thickness measured after immersion in 1.5M NaCl. f : Water uptake measured after immersion in water. g: Area resistance measured via EIS in Swagelok-style cells in 1.5 M NaCl. h: Area resistance measured via EIS+DC in 0.5 M NaCl. i: Membrane potential measurement between 0.5M and 0.1M NaCl. j : Measured after immersion in milliQ water for 24h. k : Measured in 0.005 M NaCl. l : Membrane potential measurement between 10−4M and 10−2M NaCl. m: Area resistance measured via EIS in an AORFB at SOC 50. n: Membrane potential measurement between 0.5 M and 4 M NaCl. The membrane pretreatment process (typically being counter-ion exchange and swelling of the membrane) depends on the type of membrane and counter-ion involved. For instance, some commercial AEMs are available in Br^- ion form and usually are immersed overnight in KOH or NaCl to convert them into OH^- ion or Cl^- ion form, respectively, depending on the counter-ions involved in the electrochemical reaction.

2.3 Stability

2.3.1 Chemical stability

The chemical stability of a membrane in the given electrolyte and condition can be studied by comparing the performance and structure of the membrane before and after immersing the membrane in the prepared solution for a certain period of time. Microscopic and mechanical properties comparison can be done to investigate and study possible morphological and mechanical degradation of the membrane. Another way is to compare the membrane's IEC and conductivity before and after the immersion.

Additionally, long term investigation of electrolyte-membrane interaction should be studied for a possible reactivity between certain active groups. There are various mechanisms in which a reaction between the electrolyte/redox-active species and the membrane could take place. One possible way is the oxidation of secondary and tertiary amines groups present in the membrane by the nitroxyl radicals, as shown in Figure 3 [72]. Indeed, the color of an AEM prepared using 1,4- diazabicyclo[2.2.2]octane (DABCO) with free tertiary amine groups was changed into brown after a cell test in a N,N,N-2,2,6,6-heptamethylpiperidinyl oxy-4-ammonium chloride (TMA-TEMPO)/dimethyl viologen (MV)-based AORFB [73]. The color change could be due to the oxidation of the tertiary amines of DABCO by the nitroxyl radical TMA-TEMPO. However, no changes in the membrane structure were observed via ^{1}H NMR and ATR-FTIR spectroscopy and this was assumed to be due to limited reaction and a too small amount of amine modification after only 100 cycles to be detected by such analyses.

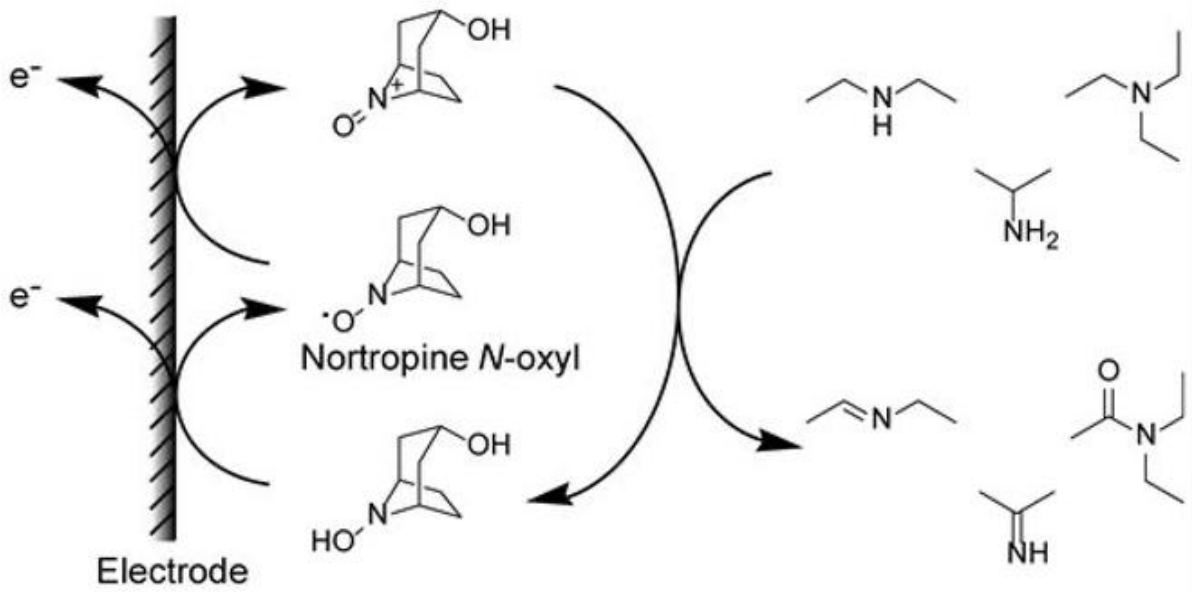

Figure 3: Electrochemical reactions of nortropine N-oxyl with different amines [72].

Similarly, an intense visual discoloration of Nafion® (NR212) membrane after cycling in an AORFB based on dihydroxyphenazine sulfonic acid (DHPS) was reported in the literature [74]. This was suggested to be due to a possible reactivity of DHPS with the Nafion® or crossover of the species through the membrane inducing capacity fade. As a result, an increase in the membrane resistance after cycling was reported.

2.3.2 Mechanical stability

Membranes must be mechanically robust, as punctures or tears of the membrane may result in rapid battery failure [75]. In RFB systems where dendrite formation is possible, such as the zinc-iodine RFB [76] or the all-copper RFB [77], metallic dendrites may puncture the membrane and lead to short-circuits and reservoir mixing. Few AORFB chemistries, however, are concerned by this problem (unless the system is a hybrid one). In systems with relatively high fluid viscosity (e.g., viologens), tearing of the membrane may occur through shearing associated with electrolyte flow around the membrane. The wall shear stress τ_m exerted on the membrane can be estimated via the formula

$$\tau_m = \mu_e \frac{\partial v}{\partial y}, \quad (7)$$

Where μ_e is the electrolyte viscosity, *v* its velocity in the electrode, proportional to the flow rate, and *y* is the through-plane direction, perpendicular to the membrane surface. The membrane will break if the wall shear stress applied exceeds

$$\tau_{max} = \frac{F}{A}, \quad (8)$$

where τ_{max} is the maximum wall shear stress, *F* is the force at rupture (which needs to be determined experimentally via a direct shear test) and *A* is the membrane area. However, most studies concerned with the mechanical stability of membranes in flow batteries feature tensile stress/strain curves measuring Young's modulus for different membranes [78]–[81] whereas tensile and compression stresses have been shown to be a concern for other parts of the stack [82]. While a linear relationship between the Young modulus and shear modulus can be justified in a RFB setup, shear tests and wall shear stress estimations should complement the assessment of the mechanical properties of membranes used in RFBs.

2.4 Estimation of membrane cost

At laboratory scale, the cost of a membrane is estimated by taking into account the cost of starting chemicals, including solvents [59]. This may give useful comparisons, the cost of M-S-TMA [73] and a membrane based on poly(phenylene) oxide) (PPO) and trimethylamine (TMA) (referred to as "Q-PPO") [59] were estimated at 425 €.m^{-2} and 8.74 €.m^{-2}, respectively. However, the PPO was supplied by different producers, and the calculation was based on the price of different amounts of PPO, perhaps hoping to account for economy of scale by assuming bulk prices of starting materials. In practice, however, the cost of other utilities, such as equipment, operations (filtration), and electricity, is frequently overlooked and would lead to a significant cost increase in the production of membranes at a larger scale. For more information on the scale-up of membrane production and associated cost estimations, the readers are suggested to refer to Minke et al. [83] for detailed calculations at the lab-scale and Xi et al. [84] at the commercial level.

Among commercially available membranes, Nafion® cation-exchange membranes exhibit the best performance, but are rather costly. Less costly alternatives exist among AEMS, such as the Fumatech® ranges, which are about 30-70% cheaper [69] or porous membranes, by far the cheapest at only 5%-10% of Nafion®'s cost [85], but which also usually exhibit significantly lower conductivity and permselectivity, or are only suitable in chemistries with large active molecules. Since the high cost of Nafion® may hinder the large-scale application of RFBs according to Zhou et al. [86], more research effort can be focused on recycling Nafion® membranes [87]. Similar recycling techniques for recovering and reusing the polymer backbone and/or ionic functions of membranes used in RFBs may be investigated in the future. Since the final cost of a membrane is determined by both the raw materials used and the synthesis procedures, low-cost and environmentally friendly materials and processes should be used.

The next section will highlight the correlation between membrane characteristics and battery performance, as well as the requirements put forward by the European Commission in terms of expected battery characteristics for stationary storage by 2030.

3. Correlating membrane properties with key battery performance indicators

In its 2020 Strategic Research Agenda for Batteries [88], the European Commission outlined Key Performance Indicators (KPI) for stationary applications and their target values for 2030. Notably, a net improvement in battery cycle life is required (15,000 cycles), as well as improvements in energy efficiency (>97%), power density (>700$ $W.kg^{-1}$) and battery module cost (70 €.kWh^{-1}).

3.1 Levelised cost of electricity storage

The levelised cost of electricity storage (LCES) [15] is given by expressing the cost of storing and discharging one kWh in a cycle over the lifetime of the battery:

$$\mathrm{LCES} = \frac{\mathrm{CC}}{\mathrm{ENH}} \tag{9}$$

where *CC* is the capital cost of installation of the battery, *E* is its energy in kWh, *N* is the total number of cycles of the battery and *H* is the round-trip efficiency (including pumping and cooling) of a cycle. Techno-economic analyses are frequently conducted in the literature [83], [89], [90] to assess the capital cost of membranes with respect to other components of the battery. Figure 4 shows a cost calculation for a 250 kW vanadium flow battery stack, for two different membranes: a Nafion® membrane estimated at 400 €.m^{-2} and a SPEEK membrane estimated at 60 €.m^{-2} [90].

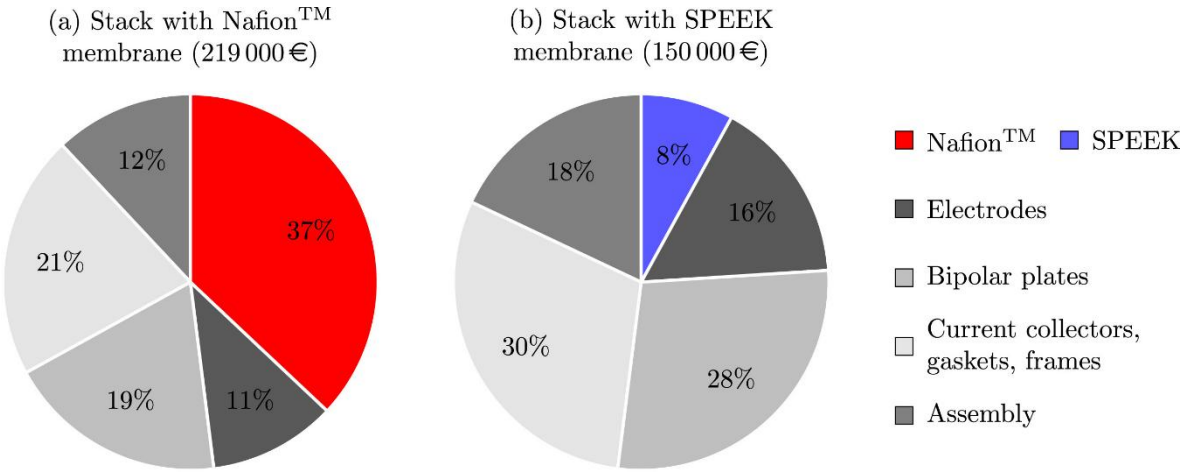

Figure 4: Cost analysis of a 250 kW flow battery stack for different membranes. Reproduced with permission from ref. [83]. Copyright Elsevier 2017.

The full analysis from Minke et al. [83] shows that the energy component of an all-vanadium battery is estimated at 390 €.kWh^{-1}. Thus, a 250 kW/MWh vanadium flow battery would cost 609 000 €, neglecting added installation and operation costs. According to Eq.(6) assuming a round-trip efficiency of 70%, the lifetime required in order to reach a levelised cost of 70 €.kWh^{-1} would amount to a minimum of 12,600 cycles, hence the 15,000 cycle lifetime target from the European Commission by 2030 [88].

Therefore, the membrane has a significant impact on the capital cost of the battery, especially in the case of Nafion®, as illustrated in Figure 4, but it also has a significant impact on the efficiency (η) and power density (in W.kg^{-1}) of the battery through its conduction properties, and on the cycle lifetime N of the battery through its separation properties. The membrane is therefore a critical component of the battery and estimating optimal trade-offs between different membrane properties is critical to the development of competitive flow batteries.

3.2 Correlating membrane ionic conduction properties with battery efficiency and power density

3.2.1 Impact of the membrane resistance on cell polarization

The cell voltage can be expressed as the contribution of three terms [91]:

$$U_{cell} = U_{OCP+} - U_{OCP-} + U_{ohmic} + \eta, \quad (10)$$

where U_{OCP} is the cell open-circuit potential, function of the composition of the reservoirs and battery state-of-charge (SoC), η is an overpotential due to Faradaic processes at the interface electrode/electrolyte (activation overpotential and concentration overpotential due to the depletion of active species [92]) and U_{ohmic} is the Ohmic drop, defined as

$$U_{Ohmic} = R_{Ohmic} I_i, \quad (11)$$

where the cell resistance R_{cell} (in Ohms) is given by the sum of different contributions

$$R_{Ohmic} = \frac{r_A}{A} + R_C + R_{DC}, \quad (12)$$

where r_A/A is the membrane resistance, usually accounting for most of the Ohmic resistance in AORFBs [70], R_C is a contact resistance between the current collector and the electrodes, and R_{DC} is an effective resistances due to ionic conduction and electronic conduction processes distributed within the electrode [93].

The polarisation behaviour of a cell relates to how the cell voltage U_{cell} (in V) and the cell power density P (in mW.cm^{-2}) evolve as a function of current density, at a constant State-of-Charge (SoC). Figure 5 shows the 0D model from Mourouga et al. [91] parametrised with a membrane Ohmic

resistance between 323 mΩ (upper red plot) and 333 mΩ (lower red plot) for the Fumasep FAA-3-50 membrane or between 250 mΩ (upper blue plot) and 270 mΩ (lower blue plot) for the in-house membrane. Experimental data points for the polarisation experiments of both membranes were performed in our lab.

Figure 5 shows the direct correlation between membrane resistance and the polarisation behaviour of a redox-flow cell. Other parameters, such as the flow rate, the temperature and the nature of the active species or the supporting electrolyte may influence the polarisation behaviour, but all these parameters taken equal, membrane conductivity and permselectivity are the main parameters influencing the polarisation behaviour of a RFB.

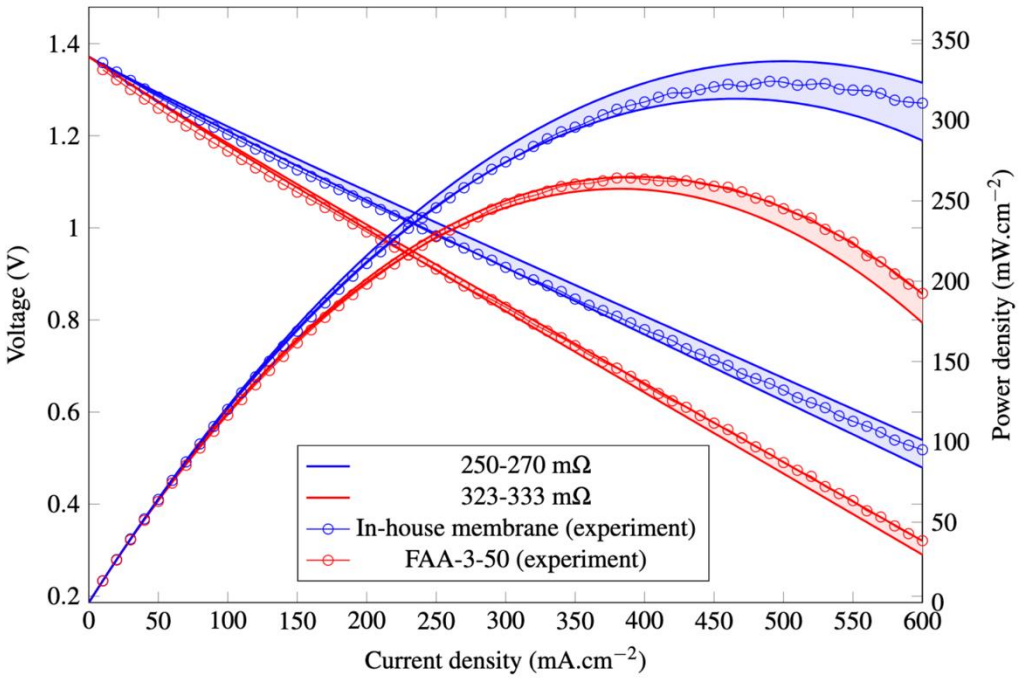

Figure 5: Comparison between the model (as described in [91]) prediction for the cell voltage and power density for different membrane conductivities, and in-house membrane polarisation experiments.

3.2.2 Battery efficiency measures

The voltage efficiency (VE) describes the effects of the polarization of the battery, which are a function of overpotentials and Ohmic drop in the cell, and is defined as

$$\mathrm{VE} = \frac{\int_{\mathrm{discharge}} \mathrm{U_{cell}(t)dt}}{\int_{\mathrm{charge}} \mathrm{U_{cell}(t)dt}}, \tag{13}$$

Fundamentally, the VE quantifies the deviation of the cell potential from its ideal open-circuit voltage which would be that of a perfectly conductive cell with no mass transport limitations. The unwanted

potentials affect the maximum state-of-charge (SoC) reachable by the battery and, in turn, its depth-of-discharge (DoD).

The Coulombic (or Faradaic) efficiency (CE) describes the charge efficiency by which electrons are transferred in batteries, and is defined as the discharge capacity divided by the charge capacity of the battery over one cycle [75]

$$\mathrm{CE} = \frac{\mathrm{Q_{discharge}}}{\mathrm{Q_{charge}}}. \quad (14)$$

Essentially, it relates to how efficiently the electronic current flowing in the current collectors translates into an ionic current through the membrane. There are two main reasons for an imperfect (<100%) Coulombic efficiency: side reactions in the electrolyte and membrane permselectivity. In the case of an imperfectly permselective membrane, the ionic current travelling through the membrane may be composed not only of the ions exchanged between the reservoirs, but also charged active material or supporting electrolyte [94].

The energy efficiency (EE) is obtained by multiplying the Coulombic and the voltage efficiencies as

$$\mathrm{EE} = \mathrm{CE} \cdot \mathrm{VE}. \quad (15)$$

The energy efficiency is therefore linked to the membrane resistance through the voltage efficiency, and the membrane permselectivity through the Coulombic efficiency, and captures the dependency of the efficiency of a cell to membrane characteristics.

Figure 6 shows the correlation between the applied current density (in $mA.cm^{-2}$) and the energy efficiency of a redox-flow cell. Experimental data for the Selemion membranes were taken from Table S1 of [95], where the electrolyte was composed of 0.5 M (ferrocenylmethyl)trimethylammonium chloride (FcNCl)/MV in 2.0 M NaCl supporting electrolyte, while the model data for the Fumasep membrane were taken from [91] where the electrolyte was composed of 1.12 M TMA-TEMPO / 1.49 M MV without supporting electrolyte. The different reservoir composition could slightly affect the energy efficiency measured in [91] and [95], but the membrane Ohmic resistance remains the primary influencing parameter, as evidenced by the comparison between Selemion membranes from Hu et al. [95].

In lithium-ion batteries, the round-trip efficiency *H* can be calculated from the energy efficiency EE of the battery, by substracting the energy consumed by the cooling system and the Battery Management System (BMS). This leads to a round-trip efficiency around 95% [96]. In RFBs, the energy spent pumping the fluid from the reservoirs to the electrodes also needs to be accounted for, which usually lowers the round-trip efficiency to about 75% [96].

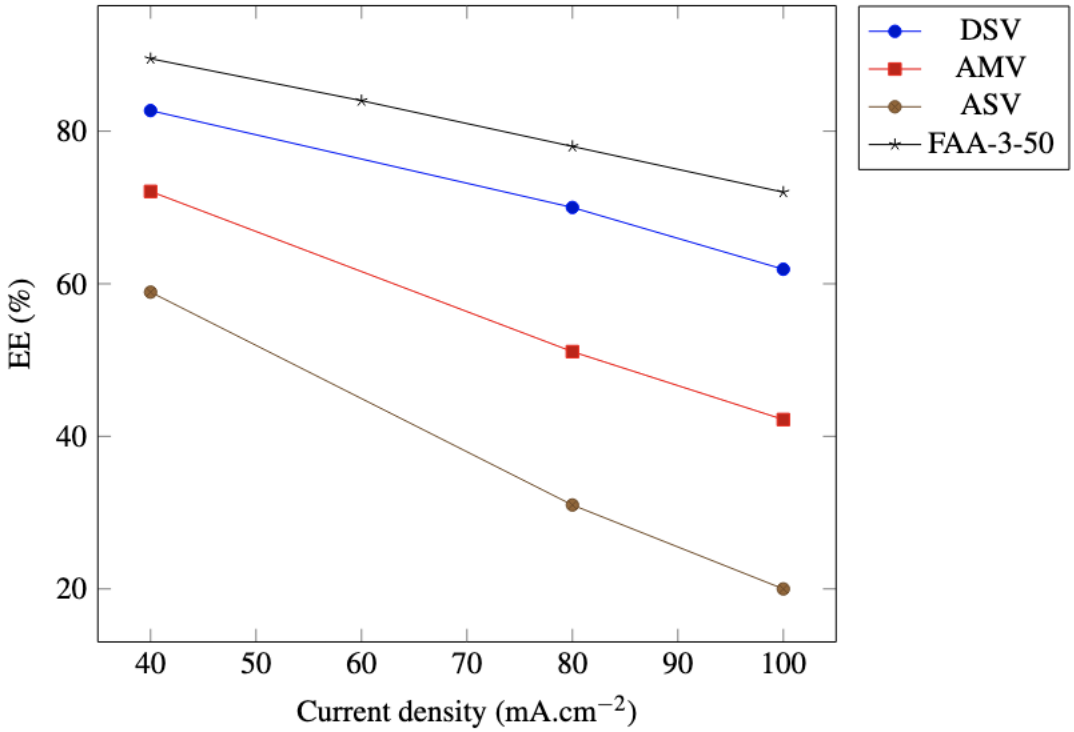

Figure 6: Plot showing the correlation between the energy efficiency and the cell current density, for different membranes. Data for Selemion (DSV, ASV, AMV) membranes were taken from Table S1 of [95] while data for the Fumasep FAA-3-50 were taken from [91].

3.3 Correlating membrane separation properties with battery lifetime

Because of the multiple causes of capacity fading, the capacity fade specifically due to membrane transport is often studied ex situ, typically through membrane permeation experiments, although as mentioned in section 2, it is not always straightforward to predict cell lifetime from simple ex situ measurements using only Fick's law. This section will focus on giving an overview of the theories of transport which were applied to membranes in flow batteries, from the first investigations to the most recent and most complete.

3.3.1 Water transfer

The first investigations of transport phenomena in RFBs focused on the membranes were done by the group of Skyllas-Kazacos in 1997 [97] and 2003 [98] and were applied to the transport of water through a Nafion membrane for the all-vanadium system. The first mechanism of water transfer identified was the osmotic flux, which is proportional to the difference in osmotic pressure between the reservoirs $P_2 - P_1$ (Pa) and was calculated by Mohammadi et al. [97] according to the ratio of the activity of water (a_w) on both sides of the membrane, which is inversely proportional to the concentration of ions,

$$P_2 - P_1 = \frac{RT}{\overline{v}_w} \ln\left(\frac{a_{w1}}{a_{w2}}\right), \quad (16)$$

where $\overline{v}_w$ is the molar volume of water (L.mol^{-1}), R is the ideal gas constant (J.kg^{-1}.K^{-1})) and T the absolute temperature (K).

A second mechanism, referred to as "hydration transfer" was also measured by Mohammadi et al. [97], and found to be proportional to the electric current density $\vec{J}$ in the battery. This transfer was attributed to the hydration shell of ions travelling through the membrane, proportional to the electro-osmotic drag coefficient of water ξ_0

$$\vec{N}_{hydration} = \frac{\xi_0}{F}\vec{J}. \quad (17)$$

Water transfer was found to be significant in the AORFB literature [69] and often, occurring even in the case where the ionic strength of the solutions was equilibrated on both sides of the membrane. This would seem to indicate that the water activities in Eq.(16) can hardly be approximated using concentration values.

3.3.2 Permeation and Fick's law

The first studies on the permeation of active species through the membrane in operating vanadium flow batteries were done by Xi et al. (2008) [99] and Sun et al. (2010) [100] and featured concentration monitoring of the reservoirs as a function of time using a dialysis cell. The use of a simple Fick's law, however, only allowed the authors to measure the permeability of the membrane to the solutes (e.g., vanadium chloride) without decoupling the effect of migration and diffusion in an operating flow battery. Batteries being subject to important electric fields, the contribution of migration and membrane permselectivity should also be accounted for.

3.3.3 The Schlögl-Nernst-Planck (SNP) equation

Fick's law was extended by Nernst's demonstration in 1888 [101]on the diffusion of charged ions and the apparition of an electric field concurrent with charge separation:

$$\overrightarrow{N_i} = -\left[D_i \nabla c_i + \frac{F}{RT} z_i D_i c_i \nabla\phi - c_i \vec{v}\right], \quad (18)$$

where D_i is a single-ion diffusion coefficient (not to be confused with solute diffusion coefficient, as it takes into account both the permeability and the permselectivity of the membrane), c_i the concentration of individual ions, z_i their valence, F is Faraday's constant, R the ideal gas constant, T the absolute temperature, ϕ the electric potential and $\vec{v}$ is a convective velocity, introduced by Shlögl in the 1960s [102] in his "extended Nernst-Planck equation" as:

$$\vec{v} = \frac{k}{\mu}[F z_R c_R \nabla\phi - \nabla p], \quad (19)$$

where k is the hydraulic permeability of the membrane (m^2), μ the dynamic viscosity of the electrolyte ($kg.m^{-1}.s^{-1}$), c_R refers to the number of charged groups per unit volume of membrane (the IEC in $mol.m^{-3}$), z_R their valence and p is hydrostatic pressure in the reservoirs (Pa).

Between 2008 and 2015, many publications on flow battery modelling (with an emphasis on membrane transport) featured finite elements models developed on the COMSOL software by Shah et al. [103], [104], than Knehr [105], [106] Wandschneider [107], Yang [108] and Lei [109] or on ANSYS fluent by Oh [110], [111]. These models featured the Schlögl-Nernst-Planck equation to model the diffusion of vanadium ions and water molecules through Nafion membranes in the all-vanadium system, however the direct use of permeability coefficients reported by Xi et al. (2008) [99] or Sun et al. (2010) [100] is surprising, as the permselectivity of the membrane to Vanadium ions should also have been measured in order to calculate the value of single-ion diffusion coefficients D_i in Eq.(19) from the values of permeability coefficients. The discrepancy between chosen values and real single-ion diffusion coefficients values may explain the lack of validation experiments in the aforementioned papers. In the meantime, the group of Skyllas-Kazacos at UNSW developed dynamic, 0D or 1D models (spatially-averaged within the electrodes) on the basis of conservation of mass and energy to observe the changes in concentrations. These models also included both ion and water transfer through the membrane [112], [113] at different temperatures [114] for Selemion® membranes (both cation-exchange and anion-exchange) and Nafion® membranes, using the Schlögl-Nernst-Planck equation. A study by Boettcher in 2015 [115] focused on reconciliating the two approaches, by comparing a 2D transient, finite element model with a 0D spatially-averaged model and concluded that the 0D approach was interesting since the loss in accuracy was relatively small, while the gain in computational efficiency was significant.

There are several issues, however, with the application of the SNP equation to flow batteries: first, the initial demonstration of Nernst [101] did not take in account an ionic current passing through the membrane due to electrochemical reactions, so that the $\Delta\phi$ term might not be as straightforward as assumed by some authors, e.g., Small et al. [57]. Second, as also mentioned by Nernst, it is rigorously only valid for very dilute solutions (<1 mM) where the ions and the membrane can be assumed not to interact electrostatically between each other, which is a very questionable hypothesis in flow battery solutions. Third, it gives very little insight into the physical origin of driving forces such as osmotic pressure, partly due to the hypothesis of infinitely dilute solutions. Fourth, as previously mentioned, single-ion diffusion coefficients involve both membrane permeability and permselectivity, and their measurement is not as straightforward as assumed by some authors in their models. Most of the papers cited above featured very little experimental validation (usually only voltage curves measured during galvanostatic charge/discharge experiment, which give little insight into transport in the battery), perhaps pointing towards limitations of the Schlögl-Nernst-Planck equation in its simplest form.

3.3.4 Modifications of the Schlögl-Nernst-Planck equation

According to Gandomi (2016) [116]*"using dilute solution theory provides diffusion data of limited utility unless a broad range of operating conditions is investigated"* which led his group to modify the Nernst-Planck equation by introducing the gradient of chemical potential of water $\Delta\mu_0$ (at the origin of osmosis), the electro-osmotic drag of water ξ_0, and most importantly introduced an interaction coefficient Θ to account for the friction between different ionic species in the membrane, potentially slowing down transport during cross-diffusion of charged species. In terms of experimental validation, their work also featured in-operando UV-visible spectroscopy, allowing for in-situ measurements of solute concentration in the reservoirs and better characterisation of the transport processes in the battery than we solely battery performance indicators (voltage, current, capacity).

In 2018, Lei [117] improved a publication from 2015 [109] using the SNP equation by introducing selective adsorption of ions inside the membrane, leading to the calculation of volume-averaged and pore-averaged ion concentrations inside the membrane, which allowed to model transport flux, in an operating all-vanadium battery more accurately and closer to experimentally measured values. In 2019, Hao [118] included interface phenomena between the membrane and the electrolyte phase within the porous electrodes, also mentioning concentrated solution effects and attempting to account for viscosity effects. Oh et al. [119] also improved upon publications from 2015 [110] and studied water transfer more accurately by introducing water activity in the membrane phase, and water content-dependent diffusivities. Experimental validation included in-operando water transfer measurements in an all-vanadium flow battery at different current densities.

The variety of modifications to the Nernst-Planck equation between 2016 and 2019 illustrates how the initial demonstration of Nernst [101] and Schlögl [102] (demonstrated for other applications) failed to accurately capture some of the phenomena at play in flow batteries, and prompted authors to return to the fundamentals of transport behind these demonstrations and explore other theories and modelling approaches, which are presented in the next section.

3.3.5 Multicomponent diffusion

The first attempt to apply concentrated solution theory to membrane transport in the all-vanadium system was done in 2014 by Gandomi et al. [120] through multicomponent diffusion theory, based on the Stefan-Maxwell diffusion equation, as applied to membranes by Pintauro in 1984 [121] and more recently Delacourt in 2008 [122]. This theory expands on the previous frameworks of diffusion by accounting for interactions between ions that are diffusing using multicomponent diffusion coefficients D_{ij}

$$c_i \Delta\mu_i = \sum_i \frac{RT c_i c_j}{c_T D_{ij}} \left(v_j - v_i\right), \quad (20)$$

where c_i is the concentration of a given specie in the membrane, $\Delta\mu_i$ its difference of chemical potential across the membrane, v_i its velocity and c_T the total concentration of species in the membrane.

This approach allows to account for the interactions between the different ions in the membrane, similarly to the reduced interaction coefficients Θ introduced in the Nernst-Planck equation by Gandomi (2016) [123], although multicomponent diffusion can be considered more complete and thermodynamically more rigorous. On the other hand, it is also more computationally and experimentally heavy, the number of parametrization experiments required to measure the diffusion coefficients D_{ij} rising rapidly as a function of the number of ionic species being transported through the membrane. In the case of Vanadium flow batteries, as underlined by Gandomi (2016) [123] *"The application of concentrated solution theory, although more accurate, is cumbersome since it requires 28 binary diffusion coefficients to be determined".* Multicomponent diffusion was nevertheless applied to vanadium flow batteries in 2020 by Crothers in a series of papers [124]–[126] which feature a very rigorous derivation of transport in concentrated, multicomponent systems of ionic species diffusing in membranes. Parts I [124] and II [125] of their theoretical derivation discuss calculation of the chemical potentials and the multicomponent diffusion coefficients D_{ik} as a function of the concentration and water content as well as membrane equivalent weight and the modulus of the hydrophobic matrix of a dry membrane. Part III [126] focuses on the validation of the demonstration on an operating all-vanadium redox-flow battery, leading to the development of the following equation of transport

$$\overrightarrow{N_i} = \frac{t_i}{z_i F} \vec{J} - \sum_k D_{ik} \nabla c_k, \quad (21)$$

where $\overrightarrow{N_i}$ is the flux of a given specie I through the membrane, t_i its transport number (proportional to the permselectivity of the membrane with respect to this specie), z_i its valence, $\vec{J}$ the operating current density of the cell and ∇c_k is the gradient of concentration across the membrane.

The flow battery model, however, lacks proper parametrization for the Vanadium ions, as mentioned by Crothers [126] "*Unfortunately, there are relatively few measurements of vanadium thermodynamic and transport properties in all its oxidation states at well-defined conditions*". A second limitation underlined by Crothers [126] is the consideration of *"a reference VRFB system containing electrodes at a fixed composition and a membrane with fixed properties"* which implies the application of the model to a battery at fixed state-of-charge, limiting its applicability to the calculation of capacity fading in an operating flow battery.

Another method, molecular dynamics (MD) was developed with the advance of computational methods in the last decades [127] and aims at modelling the elementary interactions at the molecular scale in order to calculate macroscopic parameters of transport.

3.3.6 Molecular dynamics

Molecular dynamics is an approach aimed at studying interactions phenomena from a nanoscale perspective, aiming to calculate free energies of interactions between the different species present in the membrane phase. Figure 7 shows a 13 Å cubic box used in such a simulation by Intan et al. [128], which is validated through infrared spectroscopy, and can be used to go much more in details of the interaction between charged ions, water molecules and membrane charged groups.

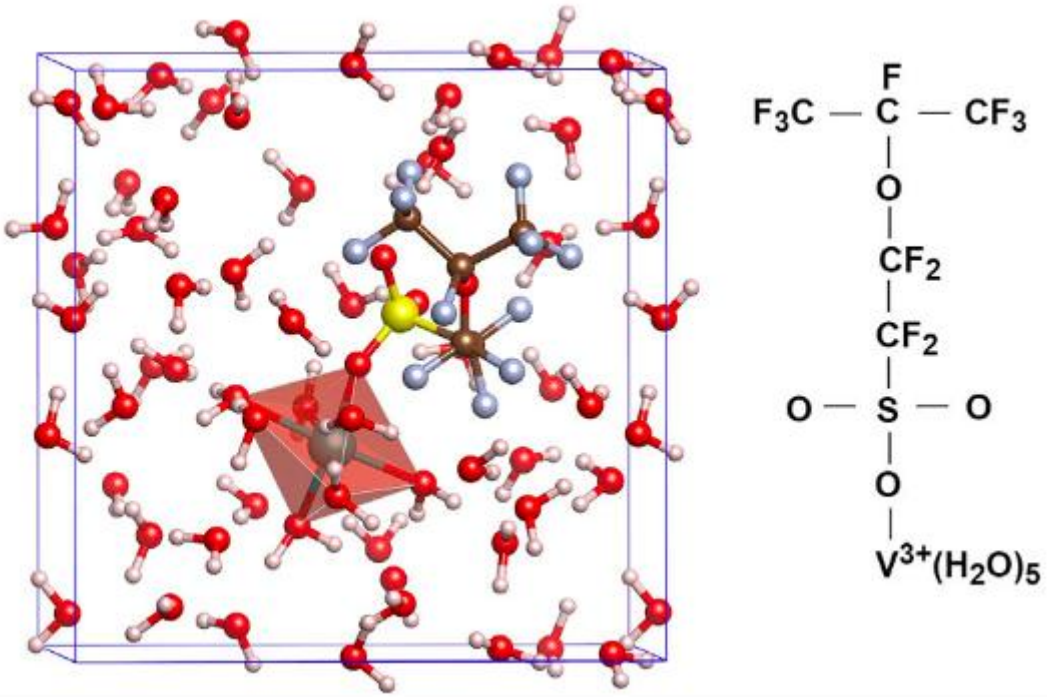

Figure 7: Cubic box of 13 Å length used in the Car-Parrinello Molecular Dynamics simulation from Intan et al. [128], aimed at studying the interactions between Nafion sulfate groups, vanadium cations and water molecules. Copyright Elsevier 2017.

While molecular dynamics can be used to calculate and even predict transport parameters more accurately, the computational cost of performing such simulation over the scale of a complete membrane in an operating flow battery would be huge, and probably unsuited to the prediction of the actual performance of the battery.

In combination with multicomponent diffusion, it could be used to model more accurately the D_{ij} coefficients, as a function of electrolyte species and membrane characteristics over a wider range of conditions than those typically used in ex-situ measurements.

3.3.7 Summary

Figure 8 shows the evolution of different equations (Schlögl-Nernst-Planck (SNP) as defined in section 3.3.3, Modified Schlögl-Nernst-Planck (MSNP) as defined in section 3.3.4 and other equations, which include concentrated solution models such as Maxwell-Stefan or non-equilibrium thermodynamics):

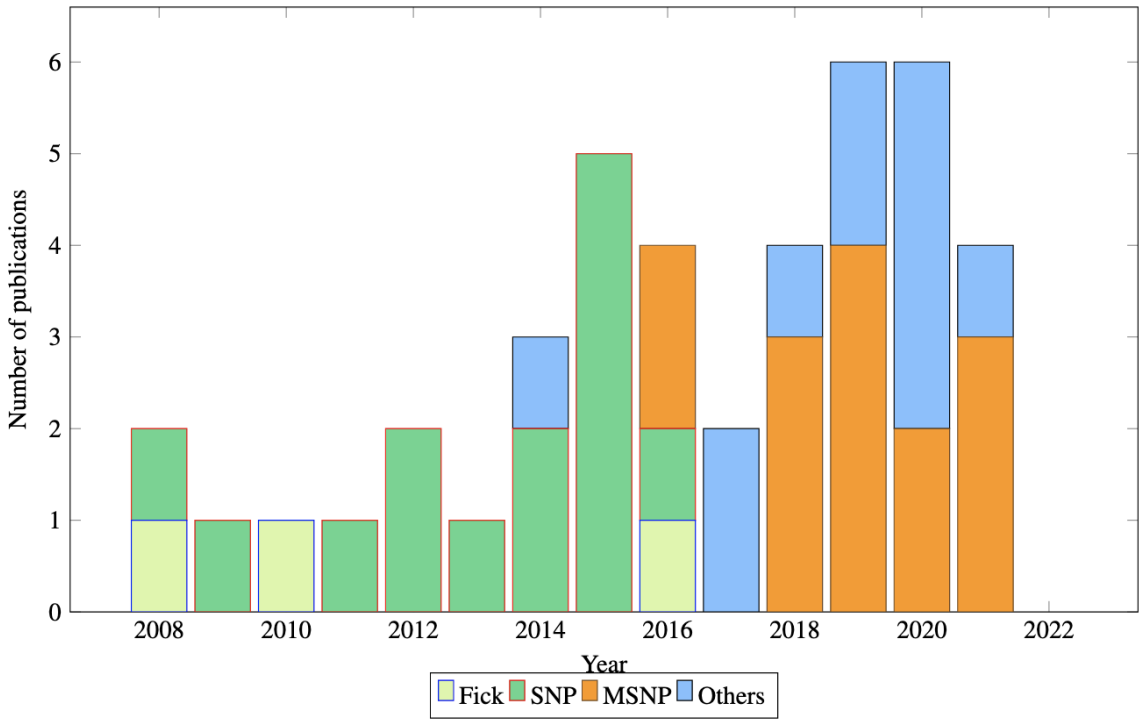

Figure 8: Illustration of the prevalence of different types of equations in the literature focusing on membrane transport processes in flow batteries. Fick: Fick's law, SNP: Schlögl-Nernst-Planck equation, MSNP: Modified Schlögl-Nernst-Planck equation, Others: Multicomponent diffusion, molecular dynamics or other sets of equation not requiring the dilute solution hypothesis.

The interesting trend to note in Figure 8 is that the Schlögl-Nernst-Planck was dominant in the early days of flow battery modelling, from 2008 to 2015, owing to its relative simplicity and low number of parameters. The experimental validation, however, was predominantly done through voltage curves of galvanostatic charge/discharge experiments and rarely featured concentration measurements in operating flow batteries, making the quantification of discrepancies between the SNP equation and actual fluxs in the battery difficult. Between 2016 and 2019, the SNP equation was modified and extended, for example by modifying the expression of the convective velocity accounting for water

transfer, or by including selective ion adsorption. Some authors, however, challenged the dilute solution hypothesis, the assumption that charged species in flow battery electrolytes (and membrane) behave like ideal gases, and favored other theories that emerged in the 20th century to model transport processes in non-ideal solutions, such as multicomponent diffusion theory, non-equilibrium thermodynamics of membrane transport processes or molecular dynamics.

The lack of proper validation and parametrization experiments in many papers from the last decade (e.g., single-ion diffusion coefficient measurements for parametrization, or capacity fading correlated with concentration and volume monitoring of the reservoirs for validation) still makes it hard to quantify the real discrepancies between models and experiments, in order to select the best modelling approaches. Nevertheless, most literature from recent years features equations in line with concentrated solution theory, which may point towards a growing consensus that once chemical potential data is made available, concentrated solution theory should emerge as a credible solution to model membrane transport processes in flow batteries and the associated capacity fading.

4. Overview of performances reported in the literature

This section, presented in three sub-sections, focuses on discussing the performance achieved for different AORFB chemistries with different membranes, both commercially available and synthesised in-house. The state-of-the-art studies on membranes for AORFBs (neutral, alkaline and acidic) is presented first, with a main focus on understanding the detailed correlations between membrane properties and cell performance. The second subsection discusses the impact of active species crossover through the membrane on AORFB capacity fade. Finally, a discussion of the trade-off between capacity fade and power density is presented, followed by a summary in a tabulated form.

4.1 AORFBs energy efficiency and power density

In 2015, Janoschka et al. [129] developed a polymerized viologen/nitroxide radical-based AORFB using NaCl(aq.) as a supporting electrolyte. Based on the large size of the active molecules, the authors favored a cellulose-based porous dialysis membrane, with a molecular weight cut-off (MWCO) of 6000 g.mol^{-1}, chosen for its low cost and compatibility with the chosen redox-active polymers [129]. The cycling performances of the polymer battery (capacity and efficiency) were reported [129], and it was observed that the discharge capacity and energy efficiency were decreased rather strongly as a function of the current density. The linear part of the decrease could be attributed to Ohmic drops in the cell, due to the membrane's relatively high area resistance, a phenomenon illustrated on Figure 9. The non-linear decrease of the discharge capacity, however, could be associated with mass transfer limitations and an increase in the overpotentials η from Eq.(10) introduced in Section 3. This would be coherent with the high molar mass of the polymer active species, leading to a slower replacement rate at the interface electrolyte/carbon fibers, at high current

densities. This, in turn, means that the maximum current density allowed by the polymer system is independent of the chosen membrane, and more strongly dependent on the size of the active molecules.

Mass transfer limitations may be what motivated Hagemann et al. [69] study's from the same laboratory, where smaller molecules, i.e., a TEMPO-based polymer as catholyte material and a simple Methyl Viologen (MV, 0.5 M) as anolyte redox-active material, both dissolved in aqueous NaCl as a supporting electrolyte, were employed. The smaller molecule size may have also motivated the choice of AEMs (Fumatech, Germany), namely the FAA-3-PE30, FAP-PK-3130, FAS-30 and FAA-3), instead of a porous dialysis membrane. The cell was cycled in a voltage window of 0.80-1.35 V as shown in Figure 9 and the capacity retention, voltage, Coulombic and energy efficiencies were plotted as a function of current density (between 1 and 16 $mA.cm^{-2}$ for the four membranes. The authors measured the cell resistance with each membrane, allowing to clearly validate the linear correlation between the variations in cell resistance associated with the different membranes and the decrease in VE with increased current density. Due to their low electric cell resistance, the cells with FAA-3-50 and FAS-30 membranes delivered a better overall battery performance than the other two systems. In particular, the FAA-3-50 membrane exhibited the lowest in-situ area resistance in agreement with its high IEC compared to other membranes, as shown in Table 2. Long-term tests were then conducted with the FAA-3-50 in order to assess the battery optimal concentration of supporting electrolyte and flow rate, as well as its lifetime due to capacity fading over time. Combined with optimized flow rate and salt concentration, the FAA-3-50-based battery exhibited an energy efficiency of 85% and Coulombic efficiency up to 95% after 100 cycles at a low current density of 5 $mA.cm^{-2}$. The main obtained performance parameters result are compiled in Table 2.

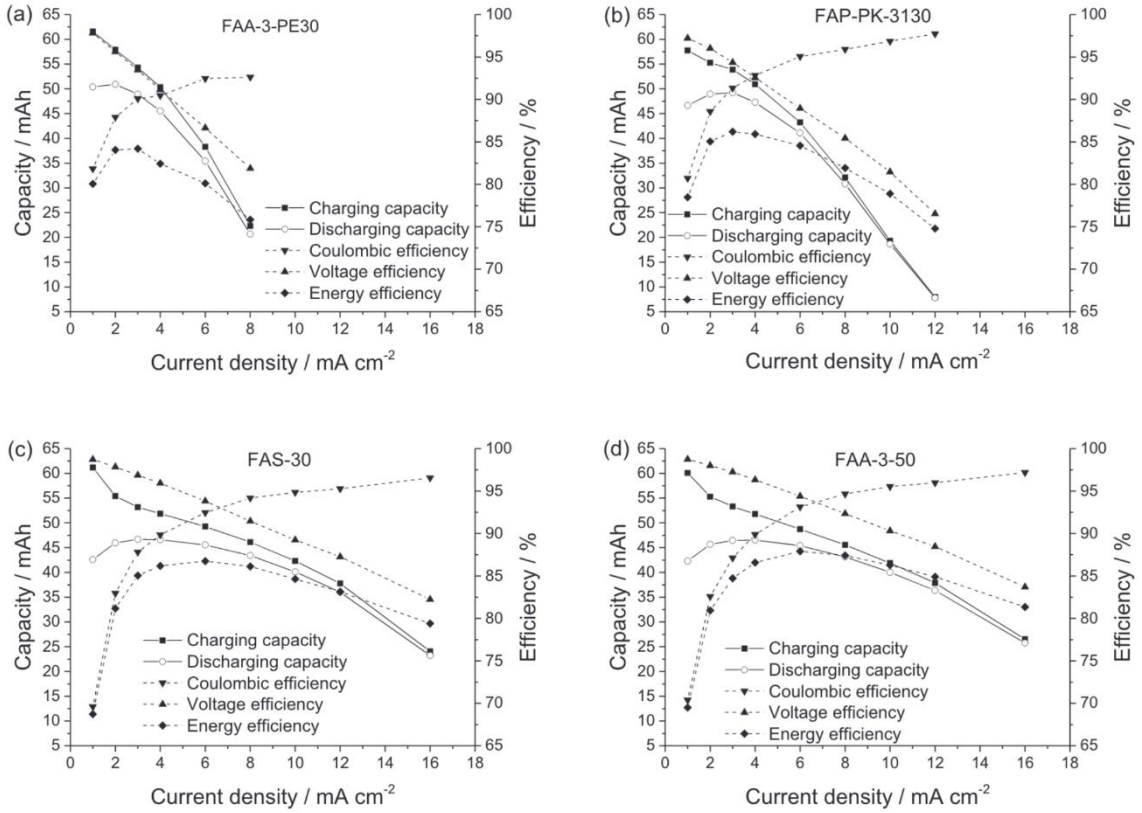

Figure 9: Battery performance of a neutral AORFB employing (a) Fumasep® FAA-3-PE30, (b) Fumasep® FAP-PK-3130, (c) Fumasep® FAS-30 and (d) Fumasep® FAA-3-50 AEM [69]. Copyright Elsevier 2017.

In another publication [95], three commercial AEMs, namely Selemion® DSV, AMV and ASV (NaCl/KCl as supporting electrolytes) with properties reported in Table 1 were tested in a neutral FcNCl/MV-based AORFB. The battery performance in terms of capacity, voltage, energy efficiencies and power density as a function of cycle number or current density for each tested membrane was reported and is summarized in Figure 10. The thinnest Selemion® DSV membrane (which exhibited the lowest cell resistance among the tested membranes) led to better battery performance: at 60 $mA.cm^{-2}$, the Selemion® DSV-employing cell exhibited higher energy efficiency (76%) than that of Selemion® AMV-based (60%) and Selemion® ASV-based (44%) cells. As shown in Figure 10d, the Selemion® DSV/NaCl-employing cell also delivered the highest peak power density of 113 $mW.cm^{-2}$ at about 200 $mA.cm^{-2}$, whereas the same cell employing AMV exhibited a much lower peak power density (66 $mW.cm^{-2}$ at 114 $mA.cm^{-2}$. These observations are coherent with the correlation between energy efficiency and measured cell area resistance shown on Figure 6.

In addition to these commercial membranes, inexpensive ($9 m^{-2}) AEM based on PPO and TMA were prepared and tested in a pH-neutral 4-[3-(trimethylammonio)propoxy]-2,2,6,6-tetramethylpiperidine-1-oxyl (TMAP-TEMPO) chloride and bis(3-trimethylammonio)propyl viologen tetra-chlorid

(BTMAP-Vi) based AORFB [59]. The Q-PPO had an IEC of 2.6 mmol.g^{-1} and water uptake of 15 wt.%. The Q-PPO-based cell exhibited an energy efficiency of 81% at a current density of 40 mA.cm^{-2} with coulombic efficiency of ≈100% for 800 consecutive cycles. Moreover, the cell delivered 95 mW.cm^{-2} at about 100% state of charge.

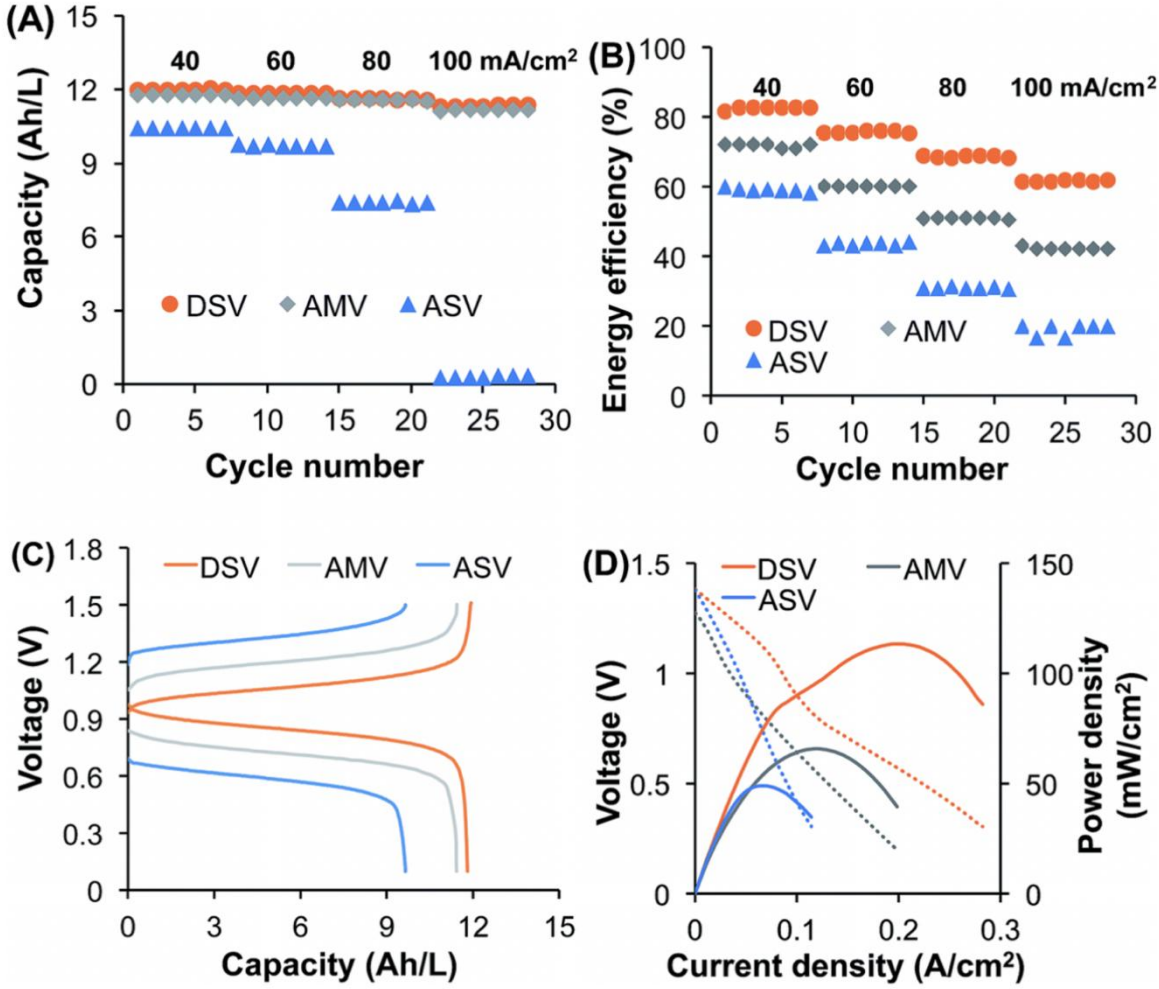

Figure 10: Neutral FcNCl/MV system with three commercial AEMs: (A) capacity vs. cycle number, (B) energy efficiency vs. cycle number, (C) Voltage profile vs. capacity at 60 mA.cm^{-2} and (D) polarization curves [95]. Copyright Royal Society of Chemistry 2014.

In alkaline AORFBs, as illustrated by the anthraquinone/ferrocyanide system from KemiWatt on Figure 1, Nafion®membranes are currently the most frequently encountered because of their high chemical stability and ion conductivity. The thickness, IEC and resistance of the most commonly used Nafion®membranes are summarized in Table 1. In these applications, membranes are usually undergoing pre-treatment [130] first, to oxidize organic contaminants, the membrane is heated in 3% H_2O_2 at 80°C for 30 min, then rinsed in deionized water. This is followed by an immersion in 1 M sulfuric acid at 80°C for 30 min in order to eliminate metallic contaminants. Finally, the membrane is rinsed with deionized water in order to remove remaining acidity. The performance of 2,5-dihydroxy-

1,4-benzoquinone (DHBQ) as a negolyte acitve species (paired with potassium ferrocyanide) for basic pH AORFBs was investigated using three different Nafion membranes - Nafion®212, Nafion®115 and Nafion®117 (denoted as N212, N115 and N117, respectively) [70]. As evidenced by polarization results (Figure 11), the DHBQ/$K_4Fe(CN)_6$ cells made with N212, N115, and N117 delivered peak power densities of 300, 164, and 137 mW.cm^{-2}, respectively. The direct current area-specific resistance (DC-ASR) of the different membranes, calculated using the derivative of the potential versus current density curve at OCV, yielded values of 1.28, 2.41, and 2.85 Ω.cm^2 for cells with N212, N115, or N117 membranes respectively, and the membrane resistance was confirmed by EIS measurements to contribute to more than 85% of the DC-ASR value. These observations are in agreement with the correlations detailed in Section 3. The performance of alkaline AORFBs employing cation exchange membranes (mainly Nafion membranes) is summarized in Table 3.

Among AORFBs in acidic conditions, quinones are reported to be an attractive class of redox-active species as they exhibit good chemical stability and rapid proton-coupled electron transfer processes, thus no precious metal catalyst is required [131]. Both hybrid (organic-inorganic) and all-organic acidic RFB systems have been demonstrated in the literature.

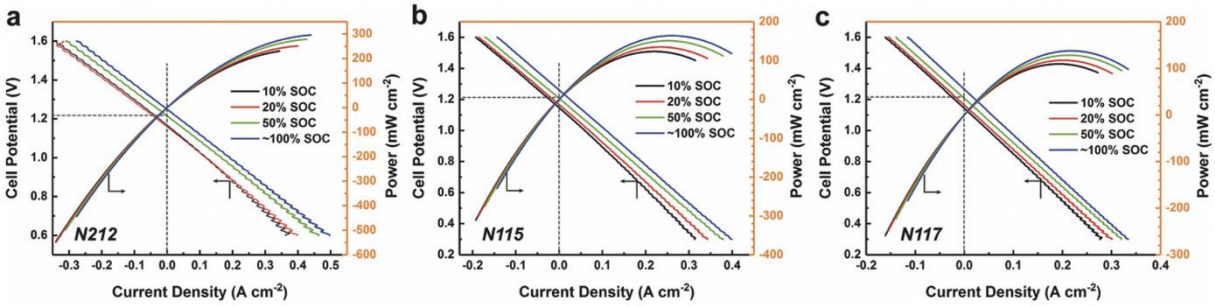

Figure 11: Electrochemical performance of a DHBQ/$K_4Fe(CN)_6$ cell assembled with a) Nafion® 212 membrane, b) Nafion® 115 membrane, and c) Nafion® 117 membrane. The dashed lines indicate OCV at 50\% SOC [70]. Copyright 2017 WILEY- VCH Verlag GmbH & Co. KGaA.

The cycling of quinone-bromide (hybrid) acidic AORFBs was first investigated by Aziz's group [132] and further developed by GES in Italy. The quinone-bromide aqueous flow battery employing Nafion®212 membrane delivered peak power density of about 600 mW.cm^{-2}. The average discharge capacity retention, after 750 deep cycles, was reported to be 99.84% per cycle. In a following study, the cell was rebuilt with N115 membrane, the average discharge capacity retention was reported to be 99.986% after cycling 106 times from near zero SOC to near 100% SOC by applying a current density of 250 mA.cm^{-2} [133]. In addition to N115 membrane's reduced water uptake (38 wt.% vs 50 wt.%) when compared to N212 membrane, the difference in cycle number could explain the variation in capacity retention. In a different study, Zhang et.al. employed Fumasep® FAP-375-PP membrane in a

phenothiazine-based (methylene blue) AORFB. The cell displayed a stable capacity for at least 900 cycles at 800 $mA.cm^{-2}$.

However, in most of the above membrane property-cell performance correlations studies, different commercial membranes are used, the chemical structure of which is unknown to the public. As a result, studying the effect of membrane IEC or thickness, for example, on cell performance would be difficult because the membranes could differ in composition and structure, as can be seen in ref.[134], in which Nafion® 212 and commercial Fumasep® E-620(K) membranes were tested in a N,N'-(9,10-anthraquinone- 2,6-diyl)-di- β-alanine/ $K_4 \backslash Fe(CN)_6$ -based alkaline AORFB. The use of membranes with the same chemical structure but different properties would be an ideal way to understand the correlation between the various membrane properties and cell cycling performance and stability, which would aid in the development of optimized membranes with high performance.

Some recent works [135] [73] featured self-made AEMs designed specifically for the neutral TMA-TEMPO/MV AORFB system. In the first work, the IEC of the AEMs was varied to modulate their water uptake and ion conductivities. The CE and EE of the cells employing the different membranes is shown in Figure 12a. The number next to the "M" refers to the IEC of the membranes. Among the tested membranes, M1.7, membrane with about 2 $mS.cm^{-1}$ Cl^- ion conductivity, 36 wt.% water uptake and low active species crossover, exhibited excellent CE (>99%) and a power density comparable to the well-performing commercial membrane (FAA-3-50) (see Figure 12b).
In the second work [73], the impact of various membrane composition and properties, such as polymer crosslinking degree, membrane thickness, cation type, presence/absence of a spacer between the polymer backbone and cation on the performance and cycling stability of the TMA-TEMPO/MV AORFB was investigated. Among these membranes, a membrane based on PPO functionalized with TMA via a 6-C spacer (M-S-TMA) because of its high Cl^- ion conductivity (4.3 $mS.cm^{-1}$ at room temperature in water), the peak power density of the cell with M-S-TMA turned out to be 293 $mW.cm^{-2}$ at flow rate of 16 $mL.min^{-1}$ (as shown in Figure 12b). On the other hand, a similar membrane (the same IEC, cation and polymer backbone) but without a 6-C spacer, M-TMA membrane, seems to be indeed affected by the absence of a flexible 6-C spacer in its structure, it exhibited a low peak power density (183 $mW.cm^{-2}$ in accordance to its lower ion conductivity (2.1 $mS.cm^{-1}$ Cl^- ion conductivity).

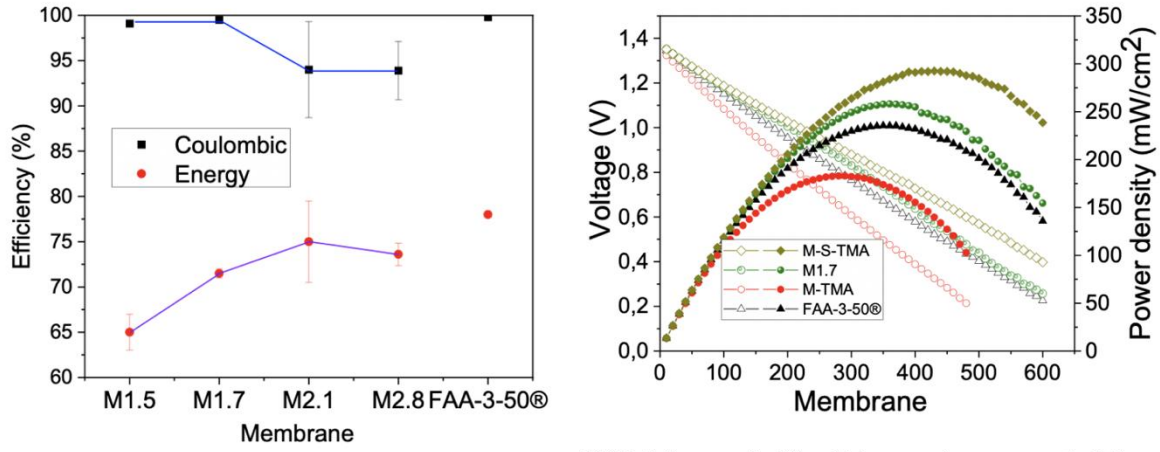

(a) Coulombic and energy efficiencies for different membranes

(b) Polarisation curves for different in-house membranes, compared with Fumasep reference

Figure 12: Correlation between IEC and cell efficiencies (a) and Polarization curves with and without 6-C spacer (b) Plots adapted from [73].

4.2 Capacity fade via active species crossover through membrane in AORFBs

Capacity fade upon cycling is one of the critical issues in AORFBs [136]. The chemical degradation mechanism and lifetime of electrolytes in AORFBs, with the main focus on capacity fade, has been discussed elsewhere [137]. In this review work, the authors classified capacity fade rates in AORFBs into extremely low (≤0.02%/day), low (0.02–0.1%/day), moderate (0.1–1%/day) and high (>1%/day) groups depending on the percentage of capacity fade per day. In order to minimize or avoid active species crossover through the membrane, one of the causes of capacity fade in AORFBs, it is important to first understand the transport mechanism of redox active species through the membranes (discussed in detailed in section 3.3) and factors affecting it.

The permeabilities of viologen-derived anolyte species such as BTMAP-Vi, bis((3-trimethylammonio) propyl) ferrocene dichloride (BTMAP-FC) and MV, usually coupled to a TEMPO-derivative posolyte, were extensively studied in the literature. Permeabilities of BTMAP-Vi, BTMAP-FC and MV through a Selemion® DSV membrane were reported (determined using Eq.(6)) to be $6.7.10^{10}$ $cm^2.s^{-1}$, $6.2.10^{-10}$ $cm^2.s^{-1}$ and $3.4.10^{-9}$ $cm^2.s^{-1}$, respectively, by Beh et al. [58]. The reduced permeabilities of the former two compounds (5 times lower than MV) across the AEM is believed to be due to their highly positively charged nature, which enhances their exclusion. The permeability of the BTMAP-Vi anolyte through another prepared PPO-based AEM was reported at 9.5. 10^{-10} $cm^2.s^{-1}$in a different study [59] while the permeability of the TMAP-TEMPO posolyte was found to be $3.4.10^{-9}$ $cm^2.s^{-1}$, more than 5 times higher. The higher diffusion coefficient for the posolyte specie was suggested to be due to

the smaller size of the TMAP-TEMPO species (crossover process accounted for 56% of the capacity fade [59].

Small et al. [57] tested five commercial AEMs (Neosepta®AFX, Neosepta® AHA, Selemion®AMV, Selemion®ASV, and Selemion®DSV) with different IEC and thicknesses in an AORFB containing N, N'-dimethyl- 4,4'-bipyridinium dichloride (Methyl Viologen) as the redox-active species in the anolyte, and 4-hydroxy-2,2,6,6-tetramethylpiperidine 1-oxyl (4-OH-TEMPO) as the active species in the catholyte [57]. The capacity fade after 100 cycles at 50 $mA.cm^{-2}$$ was mainly attributed to the crossover of the redox-active species through the membranes, due to both migration and diffusion. Membranes with higher IEC (and water uptake) displayed lower migration fluxes, indicating higher permselectivity, while membrane with lower IEC (e.g., Neosepta® AHA) displayed the lowest diffusion coefficients of active solutes. This illustrates the trade-off between conductivity, permselectivity and permeability, which can be investigated in more details through the swelling and water content of the membranes.

Similarly, in a recent study, the amount of freezable (bulky) water in AEMs was reported to be associated with TMA-TEMPO and MV crossover in AORFBs [135]. The non-freezable water molecules, which are in strong interaction with the functional group of the AEM and freezable water molecules in the membranes were determined via Differential Scanning Calorimetry (DSC). The membranes with only non-freezable water molecules were reported to have high degree of capacity retention after 103 successive charge-discharge cycles. The membranes with higher IEC (primarily M2.1 and M2.8) exhibited a high degree of active species crossover as a result of their high water uptake and freezable water molecules in the membranes (see CE values in Table 2).

Furthermore, the performance of 2,5-dihydroxy-1,4-benzoquinone (DHBQ) as a negolyte species (paired with potassium ferrocyanide in the posolyte) was investigated in basic pH AORFBs using three different Nafion membranes - N212, N115 and N117 [70]. The capacity fading of the DHBQ/$K_4Fe(CN)_6$ cell using the N212 membrane was significant (CE about 72.5% after 10 cycles). The capacity fade was believed to be caused by the DHBQ crossover through the membrane which exhibits high water uptake and small thickness, compared to the other two membranes. On the other hand, the cells employing N115 and N117 membranes exhibit an excellent CE of 99%.

In addition to ion exchange membranes, porous membranes are also used in AORFBs [129]. The cell employing cellulose-based porous dialysis membrane displayed a capacity fade rate of 0.75% per day after more than 10^4 charge-discharge cycles, consistent with the polymerized active redox species having a molecular weight three times higher than the MWCO of the porous membrane employed. However, ensuring high selectivity with such porous membranes requires polymeric or large

molecular weight redox active species. Another important aspect to consider is the power capability of the battery, together with the capacity retention when investigating the performance of a membrane in a given AORFB, since a trade-off between these two parameters is usually expected.

4.3 Trade-off between capacity fade and peak power density

As discussed in the preceding sections, the power capability and lifetime, as well as the energy efficiency, should be evaluated concurrently. While decreasing membrane thickness and/or increasing IEC tends to reduce the ohmic drop in the cell, resulting in a higher power capability, the high membrane water uptake concurrent with IEC increase, on the other hand, is detrimental to redox active species crossover. This illustrates the compromise that must be found between high power capabilities and long-term stability, related to the well-known trade-off between conductivity and selectivity reported in the membrane literature [138]–[141].

Such a compromise was illustrated by Tsehaye et al. [135]. The M1.7 membrane had a moderate IEC and a low amount of free water molecules, as evidenced by DSC results on the freezing of water-containing membranes. Similarly, M-S-TMA membrane displayed an interesting capacity retention of 84% after 100 cycles at 80 $mA.cm^{-2}$ and high peak power density in a TMA-TEMPO/MV-based AORFBs. Overall, it appears that the water uptake of the membranes should be carefully controlled without sacrificing ionic conductivity, resulting in a high-performance cell (high EE, power density and low capacity fade). According to the above two studies, membranes containing roughly 1.8 mmol $Cl^{-}.g^{-1}$ and/or membranes having a spacer between the polymer backbone and the ionic functions appear to provide a structure that allows for good conductivity and low water uptake, resulting in desirable battery performance.

The performance of neutral AORFBs employing the different membranes is summarized in Table 2, which contains reported battery performance in terms of EE, CE, VE, peak power density and cycle numbers. Only a small number of AEMs are reported, as seen in Table 2. However, in order to properly utilize these energy storage devices, appropriate membranes must also be developed and optimized. In section 5, a few points on how to achieve these aims are discussed. Moreover, standardizing testing protocols and reporting conventions would greatly help with respect to enabling proper comparisons across different systems using different membranes [142].

Table 2 : Cell performance of neutral AORFBs using different membranes.

Neutral AORFBs							
Membrane	**Redox couple**	**Nominal voltage (**V)	**Cell resistance (**$\Omega.cm^2$**)**	**Cycle number**	**Capacity retention per cycle (%)**	**Efficiency and power density**	**Ref.**
Selemion® DSV	BTMAP-Vi/BTMAP-Fc, (0.75 M/1.0 M)	0.7	2.5	500	99.9989	60 $mW.cm^{-2}$ at 150 $mA.cm^{-2}$	[58]
Selemion® AME	MV/4-HO-TEMPO in 1.5 M NaCl (0.5 M/0.5 M)	1.1 V	-	100	99.88	CE ~ 100%, EE : 62.5% at 60 $mA.cm^{-2}$	[143]
Selemion® AMV	FcNCl or FcN_2Br2/MV in 2 M NaCl (0.5 M/0.5 M)	1.0	2.9	700	99.987	~ 125 mW cm^{-2} EE : 60% (at 60 $mA.cm^{-2}$)	[144]
Selemion® DSV	FcNCl/MV in KCl	0.8	1.6	200	99.955	EE: 79% at 60 $mA.cm^{-2}$ ~ 122.7 $mW.cm^{-2}$	[95]
Selemion® AMV			3.46		99.971	EE: 66% at 60 $mA.cm^{-2}$ ~ 74.1 $mW.cm^{-2}$	

Selemion® ASV			5.87		99.961	EE: 48% at 60 $mA.cm^2$ ~ 67.2 $mW.cm^{-2}$	
Selemion® AMV	[(NPr)2V]Br_4/FcNCl in NaCl	1.38		100	99.99	92 $mW\ cm^{-2}$ CE : > 99% EE :59% at 60 $mA.cm^{-2}$	[145]
	[(Me)(NPr)V]Cl_3/FcNCl	1.38		100	99.82	CE :> 99%, EE : 65% at 60 $mA.cm^{-2}$	
FAA-3-50®	TEMPO containing copolymer/MV in 1.5 M NaCl (0.5 M)	1.075	1.67	100		CE ~ 95%, EE : 85%	[69]
Selemion® DSV	TEMPO/MV in 1.5 M NaCl	1.1	1.16*	100		100^{th} cycle, VE ~76%	[57]
Selemion® AMV			2.27*			100^{th} cycle, VE ~62.5%	
Neosepta® AFX			1.24*			100^{th} cycle, VE ~76%	
Selemion® ASV			4.76*			100^{th} cycle, VE ~50%	

Neosepta® AHA			4.81*			100th cycle, VE ~49%	
Nafion 212®	$(SPr)_2V$/KI	1.0 V	3.25	100	99.99	67.5 $mW.cm^{-2}$	[146]
Selemion CSO		1.0 V	2.26	100		EE : 67% at 60 $mA.cm^{-}2$, 92.5 $mW.cm^{-2}$	
Selemion® AMV	TMAP-TEMPO (0.1 M)/BTMAP-Vi (0.1 M)	1.1	2.2	1000	99.993	99 mW/cm^2 at 162.7 $mA.cm^{-2}$ and EE :~ 75% at 40 $mA.cm^{-2}$	[147]
FAA−3-50	TMA-TEMPO/MV	1.2	1.3	100	99.95	Peak power density : 254 $mW.cm^2$ and EE: 78% at 80 $mA.cm^{-2}$	[135]
M1.5			3.4		99.985	EE: 65% at 80 $mA.cm^{-2}$	
M1.7			2.1		99.88	EE: 71.5% at 80 $mA.cm^{-2}$	
M2.1			0.93		99.49	EE: 75% at 80 $mA.cm^{-2}$ and peak power density 258 $mW.cm^{-2}$	
M2.8			0.67		99.29	EE: 74% at 80 $mA.cm^{-2}$	

M-TMA			2.65		99.97%,	Peak power density 183 $mW.cm^{-2}$, EE: 69% at 80 $mA.cm^{-2}$	[73]
M-S-TMA			1.3		99.94%	Peak power density 293 $mW.cm^{-2}$, EE: 80% at 80 $mA.cm^{-2}$	

Abbreviations: 1,1′-bis(3-sulfonatopropyl)-4,4′-bipyridinium, $(SPr)_2V$, 1-methyl-10-[3-(trimethylammonio)propyl]-4,40-bipyridinium trichloride, $[(Me)(NPr)V]Cl_3$, 1,1′-Bis[3-(trimethylamonium)propyl]-4,4′-bipyridinium Tetrachloride, $[(NPr)_2V]Cl_4$ and *N*,*N*,*N*-2,2,6,6-heptamethylpiperidinyl oxy-4-ammonium chloride (TMA-TEMPO)/ dimethyl viologen (MV).

*Ex-situ membrane resistance in 1.5 M NaCl at 25 ^{o}C.

Table 3: Cell performance of alkaline AORFBs employing commercial CEMs.

Alkaline AORFBs							
Membrane	**Redox active species (anolyte/catholye)**	**Nominal voltage**	**Cell resistance ($\Omega.cm^2$)**	**Cycle number**	**Capacity retention per cycle (%)**	**Efficiency and power density**	**Ref.**
Nafion® 212	2,3-HCNQ/$K_4Fe(CN)_6$	1.05	-	100	99.94	Peak power density of 255 $mW.cm^{-2}$. EE = 68.6% at 100 $mA.cm^{-2}$	[148]
Nafion® 212	ACA/$K_4Fe(CN)_6$	1.1	-	400	99.985	EE = 76.5% at 80 $mA.cm^{-2}$ (at 55°C)	[149]
Nafion® 212	2,6-DHAQ/$K_4Fe(CN)_6$	1.2	0.625	100	99.9	EE = 84% at 100 $mA.cm^{-2}$	[150]
Nafion® 115	2,5-DHBQ/ $K_4Fe(CN)_6$	1.1	2.11	150	99.76	Peak power density = 164 $mW.cm^{-2}$ EE = 65% at 100 $mA.cm^{-2}$	[151]
Nafion® 117			2.60		99.68	Peak power density = 137 $mW.cm^{-2}$	

						EE = 56 % at 100 $mA.cm^{-2}$	
Nafion® 117	Lawsone/4-HO-TEMPO	0.9	2.56	215	99.992	EE = 75% at 10 $mA.cm^{-2}$	[152]
Fumasep® E-620K	0.5 M Bislawsone / ferri/ferrocyanide	1.0	1	~625	99.962.	Peak power density = 280 $mW.cm^{-2}$ energy efficiency of 79.3% at 100 $mA.cm^{-2}$	[153]
Nafion® 117	0.6 M NQ-SO/0.4 M FeCN	0.9		200	Capacity fade rate 0.006 Ah/L	EE = 55% at 100 $mA.cm^{-2}$ Peak power density = 90 $mW \cdot cm^{-2}$	[154]
Nafion® 117	Anthrarufin (AN)/$K_4Fe(CN)_6$	1.0	3.8	20	99.9	EE = 67% at 20 $mA.cm^{-2}$, Peak power density = 24 $mW \cdot cm^{-2}$	[155]

Abbreviations : 2-hydroxy-3-carboxy-1,4-naphthoquinone (2,3-HCNQ), 1,2-naphthoquinone-4-sulfonic acid sodium salt (NQ-S), 2-hydroxy-1,4-naphthoquinone (Lawsone), Polymer (poly(6-(1H-pyrrol-1-yl)quinoxaline), PPyQX), Alloxazine 7/8-carboxylic acid (ACA), Anthrarufin (AN), 2,6-dihydroxyanthraquinone (2,6-DHAQ), Lawsone (2-hydroxy-1, 4-naphthoquinone)

5. Guidelines for selecting and designing appropriate membranes

In order to calculate the optimal characteristics of a membrane for a given AORFB chemistry, it is important to understand the relationship between membrane characteristics (conductivity, permselectivity, water content, thickness, permeability) and battery performance (voltage, coulombic and energy efficiencies, power density, lifetime), an overview of which is provided in the first sections of this review. The next step is to convert these relationships to equations, which is the aim of physics-based models of membrane transport which we provided an overview of in section 3.3, in order to estimate these trade-offs quantitatively.

In the current section, it is attempted to provide guidelines with respect to choosing the optimal membrane for a given application, by discussing the most important criteria, as well as different membrane synthesis strategies and prospects in order to prepare membranes with higher battery performance than commercially available ones.

5.1 Selection criteria

For any system, the first selection step of the membrane is to choose between different categories of membranes:

- Porous membranes
- CEMs
- AEMs

Although seemingly straightforward, this choice can be much less obvious than it appears. The all-vanadium flow-battery for example, can be operated with either CEMs or AEMs [107], [156]. In one case, protons are exchanged through the CEM, while in the other sulfate ions are exchanged through the AEM between the reservoirs. The CEMs usually show worst separation properties in this system (vanadium ions being positively charged) but better performance (in terms of power density and voltage efficiency), and the consensus seems to be that the gain in performance outweighs the need for more frequent electrolyte rebalancing of the vanadium electrolytes due to higher crossover through the Nafion® membrane. In chemistries where electrolyte rebalancing may not be possible, the choice is usually determined directly by the charge of the active species and the carrier ion, to favour separation properties.

Once the nature of the membrane is determined, the second most important criterium to consider relates to the stability of the membrane in the electrolyte, which encompasses chemical, thermal, electrochemical and mechanical stabilities. Chemical stability includes the investigation of the

chemical structure using NMR, morphology (SEM), and ionic conductivity measurements before and after a stability test, by immersing membrane in the electrolyte (at different states of charge) for a few weeks, for instance. Electrochemical stability of the membranes during charge/discharge is also important as reactive radicals can be generated during battery operation, as described in Section 2.3.1. State-of-the-art AEMs are usually the most susceptible to chemical degradation, whereas Nafion® membranes are known to work well in both acidic and alkaline environments, and commercial porous (e.g., Celgard® 3501) and ceramic membranes have demonstrated the strongest chemical stability and are usually favored in NAORFBs [157]. The latter membranes should be tested in (alkaline) AORFBs due to their high chemical stability. Mechanical stability, as discussed in Section 2.3.2, can be evaluated by estimating the shear force undergone by the membrane during battery operation, proportional to the flow rate and fluid viscosity, and comparing with the shear modulus of the membrane, proportional to its thickness and dependent on the nature of the backbone.

Once a stable family of membrane (membranes with the same polymer backbone and cationic group) has been selected (e.g., Fumasep AEMs) the next selection step is to determine the precise membrane within this family (e.g., FAA-3-PE30, FAP-PK-3130, FAS-30 or FAA-3-50). The key here is to identify the optimal trade-off between cell performance defined in terms of power density, cell efficiency and cell lifetime, defined in terms of capacity fading (see Section 3) which usually come down to the reported trade-off between conductivity and selectivity [138]–[141] of the membrane.

Ion-exchange membranes can be mechanically reinforced to improve their dimensional stability by adding Zirconia nanoparticles to the polymer matrix [158], cross-linking the polymers [159], or adding a PTFE polymer backbone [79] or graphene [80] to make a composite membrane, or simply playing on the membrane thickness [160].

However, as previously discussed, the thickness of the membrane directly affects the Ohmic resistance and the cell performance, and adding elements with low conductivity to the membrane will usually decrease its conducting properties. Therefore, a trade-off must usually be chosen with respect to thickness, membrane conductivity and mechanical properties, especially at the stack level where shear stress are more important than at the lab-scale [161].

Finally, with respect to industrial applications the availability and cost of the membranes should be taken into account when choosing a membrane. As discussed in section 3.1, the membrane indeed contributes significantly to the cost of the stacks [83].

5.2 Use cases and improvements of porous membranes

Porous membranes can be readily used when the active species are an order of magnitude larger than the pore size of the membrane, e.g., polymers with a porous cellulose membrane of MWCO 6000 $g.mol^{-1}$ [129]. In such a situation, size exclusion serves as the primary transport/separation mechanism, the smaller charge carrier ions being able to pass but the larger active species being unable to cross the membrane. The main issue reported in such studies is usually the limited selectivity of such membranes, resulting in a lower coulombic efficiency, or the lower conductivity, resulting in a lower depth-of-discharge and power density.

Porous membranes can, however, be modified to provide improved selectivity. Modified porous membranes exhibit a combination of pore size exclusion and Donnan exclusion, the porous support providing size exclusion and mechanical support. Such membranes have been investigated in vanadium RFBs [162] and Zn-slurry air flow batteries [163]. The imidazolium-based AEMs (prepared by introducing imidazole groups into the pore walls of sponge-like poly(ether sulfone) porous membranes) in the former study had strong ion selectivity and VRFB performance (CE of 99% and EE of 86% at 80 $mA.cm^{-2}$. In the latter work, an ionomer (PPO with spirocyclic cation) coated Celgard®3501 membrane displayed improved ion selectivity compared to the pristine membrane. Similarly, Charyton et al. [164] coated a PVC-silica porous substrate with a vinyl imidazolium PPO/acrylamide copolymer and tested in vanadium RFB. The cell employing an optimized membrane delivered high EE (75.1%) matching the performance of commercial membranes (Nafion®N 115: 75.0% and Fumasep®FAP 450: 73.0%), tested in the same conditions.

In terms of cost and ion selectivity, such membranes are particularly appealing to be used in AORFBs. Interestingly, by altering the coating polymer type, IEC, viscosity and thickness, the ion conductivity and selectivity can be fine-tuned. Recently, an ion-exchange membrane for use in near neutral (pH = 9) AORFB was prepared by sulfonating a spirobifluorene-based microporous polymer (polymers of intrinsic microporosity) [165]. The cell was reported to be stable for at least 2100 charge-discharge cycles at 100 $mA.cm^{-2}$).

5.3 Use cases and improvements of AEMs

AEMs typically exhibit higher costs than porous membranes, but higher selectivity. In AORFBs, separation properties are often critical, so that it is very important to identify the sweet spot between criteria leading to high cycling performance (conductivity, selectivity) and those leading to high lifetime (permeability to active solutes).

One very impactful property of the membrane with respect to this trade-off is its IEC. In a recent work [135], membranes with different IEC were prepared and tested in an AORFBs. It was identified that IEC had a strong impact on water uptake, itself impacting conductivity and permeability. Membranes with IEC about 1.7 mmol $Cl.g^{-1}$ delivered better overall battery performance, comparable to commercially available FAA-3-50 membrane. Another modification method involves 6-C spacer [73], which results in reduced water uptake thanks to the defined length of the ionic channels, providing better ionic selectivity and battery performance in a neutral MV/TEMPTMA system. Active species crossover was addressed by controlling the membrane water uptake below 70 wt.%, resulting in CE of above 99.3%. In Lithium ion extraction from brine and seawater, the impact of membrane's nanochannel size, surface charge and morphology on Li^+ ions selectivity was also investigated [166].

The trade-off between conductivity and permeability is not always straightforward, as shown by a recent paper by Sanchez et al. [167], four ion exchange membranes (FAA-3-50, FAA-3-PE-30, FS-950 and E-630(K)) were modified using a pyrrole-based polymer via chemical in situ polymerization and the permeation of viologen derivative and TEMPOL was reduced by an order of magnitude, without significantly affecting the membranes ionic conductivity.

Moreover, similar investigation on the impact of nanochannel geometry, and the nature of materials selectivity employing aromatic multiblock ionomer membranes can be considered [168].

5.4 Use cases and improvements of CEMs

So far, Nafion® membranes appear unmatched in terms of performance in AORFBs where cations act as charge carriers. Different Nafion® references present variable thickness, and it appears that the N212 membrane (the thinnest) is only suitable in small-scale systems where membrane shearing is unlikely, and may lead to significant capacity fading over time. From the literature featured in this review, N117 appears to be the most commonly used.

The main drawback of Nafion® membranes being their cost, a pathway to improvement could be to focus on membrane recycling and/or synthesis process optimisation, as outlined in Section 2.4.

6. Conclusions

Aqueous organic redox flow batteries (AORFBs) are promising energy storage devices for various reasons, such as safety, low-cost potential and environmental friendliness of the supply chain. The last few years beheld an exciting growth in the development of aqueous organic redox flow batteries, where the number of publications and patents increased steadily year on year and startup companies, such as JenaBatteries, Kemiwatt and GES became closer to the point of industrial commercialisation.

In the past years of AORFB development, most attention has understandably been focused on redox active species research and operating parameters optimisation (such as flow rate). However, relatively little attention has been given to membrane development so far, since commercial membranes developed for acid recovery and desalination applications are still favored in large-scale applications, and it is not unlikely to see membranes becoming the next bottleneck for AORFB development and deployment in the next decade.

In order to push forward membrane research, it is proposed to apply detailed modeling and correlation studies between the various membrane properties and cell performance, in order to guide the development of innovative membrane technologies with tailored properties.

We have shown in this work that the flow battery literature is still lacking a clear understanding of the correlation between capacity fading of the battery and membrane transport processes, which would allow to calculate accurately the fluxes of different species through the membrane, based on the operating parameters of the battery.

Once a clear understanding of the correlation between membrane apparent properties (such as conductivity, permselectivity and permeability) and cell capacity retention and performance is established through validated numerical models, development of a battery with optimised operating parameters will be made possible. The next step will be to understand the relationship between more fundamental membrane properties such as IEC, water uptake, swelling degree, microstructure and/or chemical interaction with the electrolyte and the "higher-level" properties such as conductivity, permselectivity and permeability, through a mixture of membrane thermodynamics, molecular models and characterisation experiments. In this regard, it is worth noting that there's a definite need to standardize the active species permeability and AORFBs cell tests so that reported values can be compared. Without it, completely comprehending the relationships between membrane characteristics and cell performance under various testing parameters is challenging.

Once the theoretical interactions are understood, various strategies such as crosslinking, surface modification, controlling ionic channels and/or pore size could be employed to prepare and improve the performance of membranes used in AORFBs by controlling the IEC, the water uptake and the microstructure, thus allowing to tailor the membrane properties to a specific AORFB application. Indeed, preparing tailored membranes, i.e., membranes with well-controlled ionic channel sizes can result in a significant improvement of battery performance. Last but not least, in order to be in accordance with AORFB benefits with respect to other storage technologies, these membranes should be synthesized in a cheap and environmentally friendly way, by using economical raw materials and developing membrane recycling methods.

Acknowledgements

This project has received funding from the European Union's Horizon 2020 research and innovation programme under Grant Agreement no. 765289 (FlowCamp).

Bibliography

[1] J. Oliver and B. Sovacool, “The Energy Trilemma and the Smart Grid: Implications Beyond the United States,” *Asia Pac. Policy Stud.*, vol. 4, no. 1, 2017, doi: 10.1002/app5.95.

[2] M. Arbabzadeh, R. Sioshansi, J. X. Johnson, and G. A. Keoleian, “The role of energy storage in deep decarbonization of electricity production,” *Nat. Commun.*, vol. 10, no. 1, Jul. 2019, doi: 10.1038/s41467-019-11161-5.

[3] P. J. Heptonstall and R. J. K. Gross, “A systematic review of the costs and impacts of integrating variable renewables into power grids,” *Nat. Energy*, vol. 6, no. 1, Jan. 2021, doi: 10.1038/s41560-020-00695-4.

[4] T. M. Gür, “Review of electrical energy storage technologies, materials and systems: challenges and prospects for large-scale grid storage,” *Energy Environ. Sci.*, vol. 11, no. 10, 2018, doi: 10.1039/C8EE01419A.

[5] M. Park, J. Ryu, W. Wang, and J. Cho, “Material design and engineering of next-generation flow-battery technologies,” *Nat. Rev. Mater.*, vol. 2, Jan. 2017, doi: 10.1038/natrevmats.2016.80.

[6] E. Sum, M. Rychcik, and M. Skyllas-kazacos, “Investigation of the V(V)/V(IV) system for use in the positive half-cell of a redox battery,” *J. Power Sources*, vol. 16, no. 2, Oct. 1985, doi: 10.1016/0378-7753(85)80082-3.

[7] E. Sum and M. Skyllas-Kazacos, “A study of the V(II)/V(III) redox couple for redox flow cell applications,” *J. Power Sources*, vol. 15, no. 2, Jun. 1985, doi: 10.1016/0378-7753(85)80071-9.

[8] H. Chen, G. Cong, and Y.-C. Lu, “Recent progress in organic redox flow batteries: Active materials, electrolytes and membranes,” *J. Energy Chem.*, vol. 27, no. 5, Sep. 2018, doi: 10.1016/j.jechem.2018.02.009.

[9] V. Singh, S. Kim, J. Kang, and H. R. Byon, “Aqueous organic redox flow batteries,” *Nano Res.*, vol. 12, no. 9, Sep. 2019, doi: 10.1007/s12274-019-2355-2.

[10] W. Wang and V. Sprenkle, “Redox flow batteries go organic,” *Nat. Chem.*, vol. 8, no. 3, Mar. 2016, doi: 10.1038/nchem.2466.

[11] J. Winsberg, T. Hagemann, T. Janoschka, M. D. Hager, and U. S. Schubert, “Redox-Flow Batteries: From Metals to Organic Redox-Active Materials,” *Angew. Chem. Int. Ed.*, vol. 56, no. 3, 2017, doi: 10.1002/anie.201604925.
[12] J. Luo, B. Hu, M. Hu, Y. Zhao, and T. L. Liu, “Status and Prospects of Organic Redox Flow Batteries toward Sustainable Energy Storage,” *ACS Energy Lett.*, vol. 4, no. 9, Sep. 2019, doi: 10.1021/acsenergylett.9b01332.
[13] J. Noack, N. Roznyatovskaya, T. Herr, and P. Fischer, “The Chemistry of Redox-Flow Batteries,” *Angew. Chem. Int. Ed.*, vol. 54, no. 34, 2015, doi: 10.1002/anie.201410823.
[14] Y. Wang, P. He, and H. Zhou, “Li-Redox Flow Batteries Based on Hybrid Electrolytes: At the Cross Road between Li-ion and Redox Flow Batteries,” *Adv. Energy Mater.*, vol. 2, no. 7, 2012, doi: 10.1002/aenm.201200100.
[15] K. Wedege, E. Dražević, D. Konya, and A. Bentien, “Organic Redox Species in Aqueous Flow Batteries: Redox Potentials, Chemical Stability and Solubility,” *Sci. Rep.*, vol. 6, no. 1, Dec. 2016, doi: 10.1038/srep39101.
[16] S. Gentil, D. Reynard, and H. H. Girault, “Aqueous organic and redox-mediated redox flow batteries: a review,” *Curr. Opin. Electrochem.*, vol. 21, Jun. 2020, doi: 10.1016/j.coelec.2019.12.006.
[17] S. Fisher and R. Kunin, “Routine Exchange Capacity Determinations of Ion Exchange Resins,” *Anal. Chem.*, vol. 27, no. 7, Jul. 1955, doi: 10.1021/ac60103a052.
[18] D. Chen, S. Wang, M. Xiao, and Y. Meng, “Preparation and properties of sulfonated poly(fluorenyl ether ketone) membrane for vanadium redox flow battery application,” *J. Power Sources*, vol. 195, no. 7, Apr. 2010, doi: 10.1016/j.jpowsour.2009.11.010.
[19] S. Zhang, C. Yin, D. Xing, D. Yang, and X. Jian, “Preparation of chloromethylated/quaternized poly(phthalazinone ether ketone) anion exchange membrane materials for vanadium redox flow battery applications,” *J. Membr. Sci.*, vol. 363, no. 1–2, Nov. 2010, doi: 10.1016/j.memsci.2010.07.046.
[20] T. M. Lim, M. Ulaganathan, and Q. Yan, “Chapter 14 - Advances in membrane and stack design of redox flow batteries (RFBs) for medium- and large-scale energy storage,” in *Advances in Batteries for Medium and Large-Scale Energy Storage*, C. Menictas, M. Skyllas-Kazacos, and T. M. Lim, Eds. Woodhead Publishing, 2015. Accessed: Nov. 25, 2021. [Online]. Available: https://www.sciencedirect.com/science/article/pii/B9781782420132000145
[21] J. Parrondo, M. J. Jung, Z. Wang, C. G. Arges, and V. Ramani, “Synthesis and Alkaline Stability of Solubilized Anion Exchange Membrane Binders Based on Poly(phenylene oxide) Functionalized with Quaternary Ammonium Groups via a Hexyl Spacer,” *J. Electrochem. Soc.*, vol. 162, no. 10, Aug. 2015, doi: 10.1149/2.0891510jes.
[22] L. Semiz, N. Demirci Sankir, and M. Sankir, “Influence of the basic membrane properties of the disulfonated poly(arylene ether sulfone) copolymer membranes on the vanadium redox flow battery performance,” *J. Membr. Sci.*, vol. 468, Oct. 2014, doi: 10.1016/j.memsci.2014.06.019.
[23] I. C. Kim, J. G. Choi, and T. M. Tak, “Sulfonated polyethersulfone by heterogeneous method and its membrane performances,” *J. Appl. Polym. Sci.*, vol. 74, no. 8, Nov. 1999, doi: 10.1002/(SICI)1097-4628(19991121)74:8<2046::AID-APP20>3.0.CO;2-3.
[24] E. Moukheiber, G. De Moor, L. Flandin, and C. Bas, “Investigation of ionomer structure through its dependence on ion exchange capacity (IEC),” *J. Membr. Sci.*, vol. 389, Feb. 2012, doi: 10.1016/j.memsci.2011.10.041.
[25] Y. Mei, Z. Yao, L. Ji, P. H. Toy, and C. Y. Tang, “Effects of hypochlorite exposure on the structure and electrochemical performance of ion exchange membranes in reverse electrodialysis,” *J. Membr. Sci.*, vol. 549, Mar. 2018, doi: 10.1016/j.memsci.2017.12.016.
[26] N. Lakshminarayanaiah, “Transport Phenomena in Artificial Membranes,” *Chem. Rev.*, vol. 65, no. 5, pp. 491–565, Oct. 1965, doi: 10.1021/cr60237a001.
[27] J. Kamcev *et al.*, “Salt concentration dependence of ionic conductivity in ion exchange membranes,” *J. Membr. Sci.*, vol. 547, Feb. 2018, doi: 10.1016/j.memsci.2017.10.024.

[28] N. D. Pismenskaya, E. I. Belova, V. V. Nikonenko, and C. Larchet, “Electrical conductivity of cation-and anion-exchange membranes in ampholyte solutions,” *Russ. J. Electrochem.*, vol. 44, no. 11, Nov. 2008, doi: 10.1134/S1023193508110141.
[29] A. H. Galama, N. A. Hoog, and D. R. Yntema, “Method for determining ion exchange membrane resistance for electrodialysis systems,” *Desalination*, vol. 380, Feb. 2016, doi: 10.1016/j.desal.2015.11.018.
[30] P. Długołęcki, P. Ogonowski, S. J. Metz, M. Saakes, K. Nijmeijer, and M. Wessling, “On the resistances of membrane, diffusion boundary layer and double layer in ion exchange membrane transport,” *J. Membr. Sci.*, vol. 349, no. 1, Mar. 2010, doi: 10.1016/j.memsci.2009.11.069.
[31] F. Müller, C. A. Ferreira, D. S. Azambuja, C. Alemán, and E. Armelin, “Measuring the Proton Conductivity of Ion-Exchange Membranes Using Electrochemical Impedance Spectroscopy and Through-Plane Cell,” *J. Phys. Chem. B*, vol. 118, no. 4, Jan. 2014, doi: 10.1021/jp409675z.
[32] W. Zhang, J. Ma, P. Wang, Z. Wang, F. Shi, and H. Liu, “Investigations on the interfacial capacitance and the diffusion boundary layer thickness of ion exchange membrane using electrochemical impedance spectroscopy,” *J. Membr. Sci.*, vol. 502, Mar. 2016, doi: 10.1016/j.memsci.2015.12.007.
[33] H. G. L. Coster, T. C. Chilcott, and A. C. F. Coster, “Impedance spectroscopy of interfaces, membranes and ultrastructures,” *Bioelectrochem. Bioenerg.*, vol. 40, no. 2, Aug. 1996, doi: 10.1016/0302-4598(96)05064-7.
[34] P. C. Rieke and N. E. Vanderborgh, “Temperature dependence of water content and proton conductivity in polyperfluorosulfonic acid membranes,” *J. Membr. Sci.*, vol. 32, no. 2, Jul. 1987, doi: 10.1016/S0376-7388(00)85014-0.
[35] N. P. Berezina, N. A. Kononenko, O. A. Dyomina, and N. P. Gnusin, “Characterization of ion-exchange membrane materials: Properties vs structure,” *Adv. Colloid Interface Sci.*, vol. 139, no. 1–2, pp. 3–28, Jun. 2008, doi: 10.1016/j.cis.2008.01.002.
[36] L. Assumma, H.-D. Nguyen, C. Iojoiu, S. Lyonnard, R. Mercier, and E. Espuche, “Effects of Block Length and Membrane Processing Conditions on the Morphology and Properties of Perfluorosulfonated Poly(arylene ether sulfone) Multiblock Copolymer Membranes for PEMFC,” *ACS Appl. Mater. Interfaces*, vol. 7, no. 25, Jul. 2015, doi: 10.1021/acsami.5b01835.
[37] H.-D. Nguyen *et al.*, “Tailoring the Proton Conductivity and Microstructure of Block Copolymers by Countercation-Selective Membrane Fabrication,” *J. Phys. Chem. C*, vol. 124, no. 24, Jun. 2020, doi: 10.1021/acs.jpcc.0c04682.
[38] I. A. Prikhno, E. Yu. Safronova, I. A. Stenina, P. A. Yurova, and A. B. Yaroslavtsev, “Dependence of the Transport Properties of Perfluorinated Sulfonated Cation-Exchange Membranes on Ion-Exchange Capacity,” *Membr. Membr. Technol.*, vol. 2, no. 4, Jul. 2020, doi: 10.1134/S2517751620040095.
[39] F. Wang, M. Hickner, Y. S. Kim, T. A. Zawodzinski, and J. E. McGrath, “Direct polymerization of sulfonated poly(arylene ether sulfone) random (statistical) copolymers: candidates for new proton exchange membranes,” *J. Membr. Sci.*, vol. 197, no. 1, Mar. 2002, doi: 10.1016/S0376-7388(01)00620-2.
[40] R. Yang *et al.*, “Nonionic zeolite membrane as potential ion separator in redox-flow battery,” *J. Membr. Sci.*, vol. 450, Jan. 2014, doi: 10.1016/j.memsci.2013.08.048.
[41] T. Luo, S. Abdu, and M. Wessling, “Selectivity of ion exchange membranes: A review,” *J. Membr. Sci.*, vol. 555, pp. 429–454, Jun. 2018, doi: 10.1016/j.memsci.2018.03.051.
[42] F. G. Helfferich, *Ion exchange.* New York: McGraw-Hill, 1962. Accessed: Jan. 06, 2022. [Online]. Available: http://books.google.com/books?id=aUFRAAAAMAAJ
[43] Y. Ji and G. M. Geise, “The Role of Experimental Factors in Membrane Permselectivity Measurements,” *Ind. Eng. Chem. Res.*, vol. 56, no. 26, Jul. 2017, doi: 10.1021/acs.iecr.7b01512.
[44] G. S. Gohil, V. V. Binsu, and V. K. Shahi, “Preparation and characterization of mono-valent ion selective polypyrrole composite ion-exchange membranes,” *J. Membr. Sci.*, vol. 280, no. 1, Sep. 2006, doi: 10.1016/j.memsci.2006.01.020.

[45] M. A. Izquierdo-Gil, V. M. Barragán, J. P. G. Villaluenga, and M. P. Godino, “Water uptake and salt transport through Nafion cation-exchange membranes with different thicknesses,” *Chem. Eng. Sci.*, vol. 72, Apr. 2012, doi: 10.1016/j.ces.2011.12.040.
[46] G. M. Geise, H. J. Cassady, D. R. Paul, B. E. Logan, and M. A. Hickner, “Specific ion effects on membrane potential and the permselectivity of ion exchange membranes,” *Phys. Chem. Chem. Phys.*, vol. 16, no. 39, 2014, doi: 10.1039/C4CP03076A.
[47] Y. Ji, H. Luo, and G. M. Geise, “Specific co-ion sorption and diffusion properties influence membrane permselectivity,” *J. Membr. Sci.*, vol. 563, Oct. 2018, doi: 10.1016/j.memsci.2018.06.010.
[48] H. Strathmann, L. Giorno, and E. Drioli, “An Introduction to Membrane Science and Technology,” 2011.
[49] F. G. Wilhelm, N. F. A. van der Vegt, M. Wessling, and H. Strathmann, “Chronopotentiometry for the advanced current–voltage characterisation of bipolar membranes,” *J. Electroanal. Chem.*, vol. 502, no. 1, Apr. 2001, doi: 10.1016/S0022-0728(01)00348-5.
[50] R. K. Nagarale, G. S. Gohil, and V. K. Shahi, “Recent developments on ion-exchange membranes and electro-membrane processes,” *Adv. Colloid Interface Sci.*, vol. 119, no. 2, Feb. 2006, doi: 10.1016/j.cis.2005.09.005.
[51] P. Długołęcki, B. Anet, S. J. Metz, K. Nijmeijer, and M. Wessling, “Transport limitations in ion exchange membranes at low salt concentrations,” *J. Membr. Sci.*, vol. 346, no. 1, pp. 163–171, Jan. 2010, doi: 10.1016/j.memsci.2009.09.033.
[52] A. E. Kozmai, V. V. Nikonenko, N. D. Pismenskaya, O. D. Pryakhina, P. Sistat, and G. Pourcelly, “Diffusion layer thickness in a membrane system as determined from voltammetric and chronopotentiometric data,” *Russ. J. Electrochem.*, vol. 46, no. 12, Dec. 2010, doi: 10.1134/S1023193510120074.
[53] E. Volodina, N. Pismenskaya, V. Nikonenko, C. Larchet, and G. Pourcelly, “Ion transfer across ion-exchange membranes with homogeneous and heterogeneous surfaces,” *J. Colloid Interface Sci.*, vol. 285, no. 1, May 2005, doi: 10.1016/j.jcis.2004.11.017.
[54] J. Krol, “Chronopotentiometry and overlimiting ion transport through monopolar ion exchange membranes,” *J. Membr. Sci.*, vol. 162, no. 1–2, Sep. 1999, doi: 10.1016/S0376-7388(99)00134-9.
[55] R. Darling, K. Gallagher, W. Xie, L. Su, and F. Brushett, “Transport Property requirements for flow battery separators,” *J. Electrochem. Soc.*, vol. 163, no. 1, 2016, Accessed: Oct. 11, 2016. [Online]. Available: http://jes.ecsdl.org/content/163/1/A5029.short
[56] R. M. Darling, A. Z. Weber, M. C. Tucker, and M. L. Perry, “The Influence of Electric Field on Crossover in Redox-Flow Batteries,” *J. Electrochem. Soc.*, vol. 163, no. 1, 2016, doi: 10.1149/2.0031601jes.
[57] L. J. Small, H. D. Pratt, and T. M. Anderson, “Crossover in Membranes for Aqueous Soluble Organic Redox Flow Batteries,” *J. Electrochem. Soc.*, vol. 166, no. 12, 2019, doi: 10.1149/2.0681912jes.
[58] E. S. Beh, D. De Porcellinis, R. L. Gracia, K. T. Xia, R. G. Gordon, and M. J. Aziz, “A Neutral pH Aqueous Organic–Organometallic Redox Flow Battery with Extremely High Capacity Retention,” *ACS Energy Lett.*, vol. 2, no. 3, Mar. 2017, doi: 10.1021/acsenergylett.7b00019.
[59] Y. Li, Y. Liu, Z. Xu, and Z. Yang, “Poly(phenylene oxide)-Based Ion-Exchange Membranes for Aqueous Organic Redox Flow Battery,” *Ind. Eng. Chem. Res.*, vol. 58, no. 25, Jun. 2019, doi: 10.1021/acs.iecr.9b01377.
[60] M. J. Baran *et al.*, “Design Rules for Membranes from Polymers of Intrinsic Microporosity for Crossover-free Aqueous Electrochemical Devices,” *Joule*, vol. 3, no. 12, Dec. 2019, doi: 10.1016/j.joule.2019.08.025.
[61] R. Kingsbury, S. Zhu, S. Flotron, and O. Coronell, “Microstructure determines water and salt permeation in commercial ion exchange membranes,” Oct. 2018, doi: 10.26434/chemrxiv.6987248.v4.

[62] W. Xie, J. Cook, H. B. Park, B. D. Freeman, C. H. Lee, and J. E. McGrath, “Fundamental salt and water transport properties in directly copolymerized disulfonated poly(arylene ether sulfone) random copolymers,” *Polymer*, vol. 52, no. 9, Apr. 2011, doi: 10.1016/j.polymer.2011.02.006.
[63] H. Y. Elmoazzen, J. A. W. Elliott, and L. E. McGann, “Osmotic Transport across Cell Membranes in Nondilute Solutions: A New Nondilute Solute Transport Equation,” *Biophys. J.*, vol. 96, no. 7, Apr. 2009, doi: 10.1016/j.bpj.2008.12.3929.
[64] L. Yan *et al.*, “Balancing Osmotic Pressure of Electrolytes for Nanoporous Membrane Vanadium Redox Flow Battery with a Draw Solute,” *ACS Appl. Mater. Interfaces*, vol. 8, no. 51, Dec. 2016, doi: 10.1021/acsami.6b12068.
[65] J.-M. Fontmorin, S. Guihéneuf, P. Bassil, F. Geneste, and D. Floner, “Addition of weak acids in electrolytes to prevent osmosis in aqueous organic redox flow batteries,” *Electrochem. Commun.*, vol. 132, Nov. 2021, doi: 10.1016/j.elecom.2021.107148.
[66] M. Q. Gubari, H. M. Zwain, and N. V. Alekseeva, “Diffusion and Osmotic Permeability of Ion Exchange Membrane MK-40 Using Sodium Chloride Solution,” *Pertanika J. Sci. Technol.*, vol. 29, no. 4, Oct. 2021, doi: 10.47836/pjst.29.4.14.
[67] Y. Mei and C. Y. Tang, “Recent developments and future perspectives of reverse electrodialysis technology: A review,” *Desalination*, vol. 425, Jan. 2018, doi: 10.1016/j.desal.2017.10.021.
[68] R. Kingsbury, S. Zhu, S. Flotron, and O. Coronell, “Microstructure determines water and salt permeation in commercial ion exchange membranes,” Chemistry, preprint, Aug. 2018. doi: 10.26434/chemrxiv.6987248.v3.
[69] T. Hagemann *et al.*, “An aqueous all-organic redox-flow battery employing a (2,2,6,6-tetramethylpiperidin-1-yl)oxyl-containing polymer as catholyte and dimethyl viologen dichloride as anolyte,” *J. Power Sources*, vol. 378, Feb. 2018, doi: 10.1016/j.jpowsour.2017.09.007.
[70] Z. Yang *et al.*, “Alkaline Benzoquinone Aqueous Flow Battery for Large-Scale Storage of Electrical Energy,” *Adv. Energy Mater.*, vol. 8, no. 8, 2018, doi: 10.1002/aenm.201702056.
[71] A. H. Avci *et al.*, “Energy Harvesting from Brines by Reverse Electrodialysis Using Nafion Membranes,” *Membranes*, vol. 10, no. 8, Aug. 2020, doi: 10.3390/membranes10080168.
[72] K. Sato *et al.*, “Electrochemical Oxidation of Amines Using a Nitroxyl Radical Catalyst and the Electroanalysis of Lidocaine,” *Catalysts*, vol. 8, no. 12, Dec. 2018, doi: 10.3390/catal8120649.
[73] M. T. Tsehaye, “Development of anion exchange membranes for aqueous organic redox and zinc slurry-air flow batteries,” phdthesis, Université Grenoble Alpes [2020-....], 2021. Accessed: Mar. 21, 2022. [Online]. Available: https://tel.archives-ouvertes.fr/tel-03292028
[74] A. Hollas *et al.*, “A biomimetic high-capacity phenazine-based anolyte for aqueous organic redox flow batteries,” *Nat. Energy*, vol. 3, no. 6, Jun. 2018, doi: 10.1038/s41560-018-0167-3.
[75] C. A. Machado, G. O. Brown, R. Yang, T. E. Hopkins, J. G. Pribyl, and T. H. Epps, “Redox Flow Battery Membranes: Improving Battery Performance by Leveraging Structure–Property Relationships,” *ACS Energy Lett.*, vol. 6, no. 1, Jan. 2021, doi: 10.1021/acsenergylett.0c02205.
[76] C. Xie, H. Zhang, W. Xu, W. Wang, and X. Li, “A Long Cycle Life, Self-Healing Zinc–Iodine Flow Battery with High Power Density,” *Angew. Chem. Int. Ed.*, vol. 57, no. 35, 2018, doi: 10.1002/anie.201803122.
[77] D. Lloyd, T. Vainikka, and K. Kontturi, “The development of an all copper hybrid redox flow battery using deep eutectic solvents,” *Electrochimica Acta*, vol. 100, Jun. 2013, doi: 10.1016/j.electacta.2013.03.130.
[78] M. P. Rodgers, J. Berring, S. Holdcroft, and Z. Shi, “The effect of spatial confinement of Nafion® in porous membranes on macroscopic properties of the membrane,” *J. Membr. Sci.*, vol. 321, no. 1, Aug. 2008, doi: 10.1016/j.memsci.2008.01.007.
[79] W. Wei, H. Zhang, X. Li, Z. Mai, and H. Zhang, “Poly(tetrafluoroethylene) reinforced sulfonated poly(ether ether ketone) membranes for vanadium redox flow battery application,” *J. Power Sources*, vol. 208, Jun. 2012, doi: 10.1016/j.jpowsour.2012.02.047.

[80] W. Dai *et al.*, "Sulfonated Poly(Ether Ether Ketone)/Graphene composite membrane for vanadium redox flow battery," *Electrochimica Acta*, vol. 132, Jun. 2014, doi: 10.1016/j.electacta.2014.03.156.
[81] L. Yu, F. Lin, L. Xu, and J. Xi, "Structure–property relationship study of Nafion XL membrane for high-rate, long-lifespan, and all-climate vanadium flow batteries," *RSC Adv.*, vol. 7, no. 50, Jun. 2017, doi: 10.1039/C7RA04996J.
[82] J. Xiong, M. Jing, A. Tang, X. Fan, J. Liu, and C. Yan, "Mechanical modelling and simulation analyses of stress distribution and material failure for vanadium redox flow battery," *J. Energy Storage*, vol. 15, Feb. 2018, doi: 10.1016/j.est.2017.11.011.
[83] C. Minke, U. Kunz, and T. Turek, "Techno-economic assessment of novel vanadium redox flow batteries with large-area cells," *J. Power Sources*, vol. 361, Sep. 2017, doi: 10.1016/j.jpowsour.2017.06.066.
[84] J. Xi, B. Jiang, L. Yu, and L. Liu, "Membrane evaluation for vanadium flow batteries in a temperature range of −20–50°C," *J. Membr. Sci.*, vol. 522, Jan. 2017, doi: 10.1016/j.memsci.2016.09.012.
[85] T. Janoschka, N. Martin, M. D. Hager, and U. S. Schubert, "An Aqueous Redox-Flow Battery with High Capacity and Power: The TEMPTMA/MV System," *Angew. Chem. Int. Ed.*, vol. 55, no. 46, 2016, doi: https://doi.org/10.1002/anie.201606472.
[86] Y. Zhou, L. Yu, J. Wang, L. Liu, F. Liang, and J. Xi, "Rational use and reuse of Nafion 212 membrane in vanadium flow batteries," *RSC Adv.*, vol. 7, no. 32, 2017, doi: 10.1039/C7RA00294G.
[87] J. Alipour Moghaddam, M. J. Parnian, and S. Rowshanzamir, "Preparation, characterization, and electrochemical properties investigation of recycled proton exchange membrane for fuel cell applications," *Energy*, vol. 161, Oct. 2018, doi: 10.1016/j.energy.2018.07.123.
[88] European Commission, "Batteries Europe Strategic Research Agenda for batteries," 2020. Accessed: Jan. 04, 2022. [Online]. Available: https://ec.europa.eu/energy/sites/default/files/documents/batteries_europe_strategic_research_agenda_december_2020__1.pdf
[89] V. Viswanathan *et al.*, "Cost and performance model for redox flow batteries," *J. Power Sources*, vol. 247, Feb. 2014, doi: 10.1016/j.jpowsour.2012.12.023.
[90] C. Minke and T. Turek, "Economics of vanadium redox flow battery membranes," *J. Power Sources*, vol. 286, Jul. 2015, doi: 10.1016/j.jpowsour.2015.03.144.
[91] G. Mourouga, R. P. Schaerer, X. Yang, T. Janoschka, T. J. Schmidt, and J. O. Schumacher, "Physics-based 0D-U-I-SoC Cell Performance Modelfor Aqueous Organic Redox Flow Batteries," *Electrochimica Acta*, p. 140185, Mar. 2022, doi: 10.1016/j.electacta.2022.140185.
[92] N. M. Delgado, R. Monteiro, M. Abdollahzadeh, P. Ribeirinha, A. Bentien, and A. Mendes, "2D-dynamic phenomenological modelling of vanadium redox flow batteries – Analysis of the mass transport related overpotentials," *J. Power Sources*, vol. 480, p. 229142, Dec. 2020, doi: 10.1016/j.jpowsour.2020.229142.
[93] Q. Chen, M. R. Gerhardt, and M. J. Aziz, "Dissection of the Voltage Losses of an Acidic Quinone Redox Flow Battery," *J. Electrochem. Soc.*, vol. 164, no. 6, 2017, doi: 10.1149/2.0721706jes.
[94] D. Chen *et al.*, "Porous Membrane with High Selectivity for Alkaline Quinone-Based Flow Batteries," *ACS Appl. Mater. Interfaces*, vol. 12, no. 43, Oct. 2020, doi: 10.1021/acsami.0c13172.
[95] B. Hu, C. Seefeldt, C. DeBruler, and T. L. Liu, "Boosting the energy efficiency and power performance of neutral aqueous organic redox flow batteries," *J. Mater. Chem. A*, vol. 5, no. 42, Oct. 2017, doi: 10.1039/C7TA06573F.
[96] M. Steilen and L. Jörissen, "Hydrogen Conversion into Electricity and Thermal Energy by Fuel Cells," in *Electrochemical Energy Storage for Renewable Sources and Grid Balancing*, Elsevier, 2015, pp. 143–158. doi: 10.1016/B978-0-444-62616-5.00010-3.

[97] T. Mohammadi, S. C. Chieng, and M. Skyllas Kazacos, “Water transport study across commercial ion exchange membranes in the vanadium redox flow battery,” *J. Membr. Sci.*, vol. 133, no. 2, Oct. 1997, doi: 10.1016/S0376-7388(97)00092-6.

[98] T. Sukkar and M. Skyllas-Kazacos, “Water transfer behaviour across cation exchange membranes in the vanadium redox battery,” *J. Membr. Sci.*, vol. 222, no. 1, Sep. 2003, doi: 10.1016/S0376-7388(03)00309-0.

[99] J. Xi, Z. Wu, X. Teng, Y. Zhao, L. Chen, and X. Qiu, “Self-assembled polyelectrolyte multilayer modified Nafion membrane with suppressed vanadium ion crossover for vanadium redox flow batteries,” *J. Mater. Chem.*, vol. 18, no. 11, Mar. 2008, doi: 10.1039/B718526J.

[100] C. Sun, J. Chen, H. Zhang, X. Han, and Q. Luo, “Investigations on transfer of water and vanadium ions across Nafion membrane in an operating vanadium redox flow battery,” *J. Power Sources*, vol. 195, no. 3, Feb. 2010, doi: 10.1016/j.jpowsour.2009.08.041.

[101] W. Nernst, “Zur Kinetik der in Lösung befindlichen Körper,” *Z. Für Phys. Chem.*, 1888, Accessed: May 11, 2021. [Online]. Available: http://publikationen.ub.uni-frankfurt.de/frontdoor/index/index/docId/11523

[102] R. Schlögl, “Membrane permeation in systems far from equilibrium,” *Berichte Bunsenges.*, 1965, doi: 10.1002/bbpc.19660700403.

[103] A. A. Shah, M. J. Watt-Smith, and F. C. Walsh, “A dynamic performance model for redox-flow batteries involving soluble species,” *Electrochimica Acta*, vol. 53, no. 27, pp. 8087–8100, Nov. 2008, doi: 10.1016/j.electacta.2008.05.067.

[104] H. Al-Fetlawi, A. A. Shah, and F. C. Walsh, “Non-isothermal modelling of the all-vanadium redox flow battery,” *Electrochimica Acta*, vol. 55, no. 1, pp. 78–89, Dec. 2009, doi: 10.1016/j.electacta.2009.08.009.

[105] K. W. Knehr, E. Agar, C. R. Dennison, A. R. Kalidindi, and E. C. Kumbur, “A Transient Vanadium Flow Battery Model Incorporating Vanadium Crossover and Water Transport through the Membrane,” *J. Electrochem. Soc.*, vol. 159, no. 9, Aug. 2012, doi: 10.1149/2.017209jes.

[106] E. Agar, K. W. Knehr, D. Chen, M. A. Hickner, and E. C. Kumbur, “Species transport mechanisms governing capacity loss in vanadium flow batteries: Comparing Nafion® and sulfonated Radel membranes,” *Electrochimica Acta*, vol. 98, May 2013, doi: 10.1016/j.electacta.2013.03.030.

[107] F. T. Wandschneider *et al.*, “Model of a vanadium redox flow battery with an anion exchange membrane and a Larminie-correction,” *J. Power Sources*, vol. 272, Dec. 2014, doi: 10.1016/j.jpowsour.2014.08.082.

[108] X.-G. Yang, Q. Ye, P. Cheng, and T. S. Zhao, “Effects of the electric field on ion crossover in vanadium redox flow batteries,” *Appl. Energy*, vol. 145, May 2015, doi: 10.1016/j.apenergy.2015.02.038.

[109] Y. Lei, “A transient electrochemical model incorporating the Donnan effect for all-vanadium redox flow batteries,” *J. Power Sources*, 2015.

[110] K. Oh, S. Won, and H. Ju, “A comparative study of species migration and diffusion mechanisms in all-vanadium redox flow batteries,” *Electrochimica Acta*, vol. 181, Nov. 2015, doi: 10.1016/j.electacta.2015.03.012.

[111] S. Won, K. Oh, and H. Ju, “Numerical analysis of vanadium crossover effects in all-vanadium redox flow batteries,” *Electrochimica Acta*, vol. 177, Sep. 2015, doi: 10.1016/j.electacta.2015.01.166.

[112] A. Tang, J. Bao, and M. Skyllas-Kazacos, “Dynamic modelling of the effects of ion diffusion and side reactions on the capacity loss for vanadium redox flow battery,” *J. Power Sources*, vol. 196, no. 24, Dec. 2011, doi: 10.1016/j.jpowsour.2011.09.003.

[113] A. Tang, S. Ting, J. Bao, and M. Skyllas-Kazacos, “Thermal modelling and simulation of the all-vanadium redox flow battery,” *J. Power Sources*, vol. 203, pp. 165–176, Apr. 2012, doi: 10.1016/j.jpowsour.2011.11.079.

[114] R. Badrinarayanan, J. Zhao, K. J. Tseng, and M. Skyllas-Kazacos, “Extended dynamic model for ion diffusion in all-vanadium redox flow battery including the effects of temperature and bulk electrolyte transfer,” *J. Power Sources*, vol. 270, Dec. 2014, doi: 10.1016/j.jpowsour.2014.07.128.

[115] P. A. Boettcher, E. Agar, C. R. Dennison, and E. C. Kumbur, “Modeling of Ion Crossover in Vanadium Redox Flow Batteries: A Computationally-Efficient Lumped Parameter Approach for Extended Cycling,” *J. Electrochem. Soc.*, vol. 163, no. 1, Dec. 2015, doi: 10.1149/2.0311601jes.

[116] Y. Ashraf Gandomi, D. S. Aaron, and M. M. Mench, “Coupled Membrane Transport Parameters for Ionic Species in All-Vanadium Redox Flow Batteries,” *Electrochimica Acta*, vol. 218, Nov. 2016, doi: 10.1016/j.electacta.2016.09.087.

[117] Y. Lei, B. W. Zhang, Z. H. Zhang, B. F. Bai, and T. S. Zhao, “An improved model of ion selective adsorption in membrane and its application in vanadium redox flow batteries,” *Appl. Energy*, vol. 215, Apr. 2018, doi: 10.1016/j.apenergy.2018.02.042.

[118] L. Hao, Y. Wang, and Y. He, “Modeling of Ion Crossover in an All-Vanadium Redox Flow Battery with the Interfacial Effect at Membrane/Electrode Interfaces,” *J. Electrochem. Soc.*, vol. 166, no. 8, Apr. 2019, doi: 10.1149/2.1061906jes.

[119] K. Oh, M. Moazzam, G. Gwak, and H. Ju, “Water crossover phenomena in all-vanadium redox flow batteries,” *Electrochimica Acta*, vol. 297, Feb. 2019, doi: 10.1016/j.electacta.2018.11.151.

[120] Y. A. Gandomi, T. A. Zawodzinski, and M. M. Mench, “Concentrated Solution Model of Transport in All Vanadium Redox Flow Battery Membrane Separator,” *ECS Trans.*, vol. 61, no. 13, Sep. 2014, doi: 10.1149/06113.0023ecst.

[121] P. N. Pintauro and D. N. Bennion, “Mass transport of electrolytes in membranes. 1. Development of mathematical transport model,” *Ind. Eng. Chem. Fundam.*, vol. 23, no. 2, pp. 230–234, May 1984, doi: 10.1021/i100014a016.

[122] C. Delacourt and J. Newman, “Mathematical Modeling of a Cation-Exchange Membrane Containing Two Cations,” *J. Electrochem. Soc.*, vol. 155, no. 11, 2008, doi: 10.1149/1.2977960.

[123] Y. Ashraf Gandomi, D. S. Aaron, and M. M. Mench, “Influence of Membrane Equivalent Weight and Reinforcement on Ionic Species Crossover in All-Vanadium Redox Flow Batteries,” *Membranes*, vol. 7, no. 2, Jun. 2017, doi: 10.3390/membranes7020029.

[124] A. R. Crothers, R. M. Darling, A. Kusoglu, C. J. Radke, and A. Z. Weber, “Theory of Multicomponent Phenomena in Cation-Exchange Membranes: Part I. Thermodynamic Model and Validation,” *J. Electrochem. Soc.*, vol. 167, no. 1, Jan. 2020, doi: 10.1149/1945-7111/ab6723.

[125] A. R. Crothers, R. M. Darling, A. Kusoglu, C. J. Radke, and A. Z. Weber, “Theory of Multicomponent Phenomena in Cation-Exchange Membranes: Part II. Transport Model and Validation,” *J. Electrochem. Soc.*, vol. 167, no. 1, Feb. 2020, doi: 10.1149/1945-7111/ab6724.

[126] A. R. Crothers, R. M. Darling, D. I. Kushner, M. L. Perry, and A. Z. Weber, “Theory of Multicomponent Phenomena in Cation-Exchange Membranes: Part III. Transport in Vanadium Redox-Flow-Battery Separators,” *J. Electrochem. Soc.*, vol. 167, no. 1, Feb. 2020, doi: 10.1149/1945-7111/ab6725.

[127] R. M. Venable, A. Krämer, and R. W. Pastor, “Molecular Dynamics Simulations of Membrane Permeability,” *Chem. Rev.*, vol. 119, no. 9, May 2019, doi: 10.1021/acs.chemrev.8b00486.

[128] N. N. Intan, K. Klyukin, T. J. Zimudzi, M. A. Hickner, and V. Alexandrov, “A combined theoretical-experimental study of interactions between vanadium ions and Nafion membrane in all-vanadium redox flow batteries,” *J. Power Sources*, vol. 373, Jan. 2018, doi: 10.1016/j.jpowsour.2017.10.050.

[129] T. Janoschka *et al.*, “An aqueous, polymer-based redox-flow battery using non-corrosive, safe, and low-cost materials,” *Nature*, vol. 527, no. 7576, pp. 78–81, Oct. 2015, doi: 10.1038/nature15746.

[130] P. Hu *et al.*, “Renewable-lawsone-based sustainable and high-voltage aqueous flow battery,” *Energy Storage Mater.*, vol. 19, May 2019, doi: 10.1016/j.ensm.2018.10.017.

[131] B. Yang, L. Hoober-Burkhardt, F. Wang, G. K. S. Prakash, and S. R. Narayanan, “An Inexpensive Aqueous Flow Battery for Large-Scale Electrical Energy Storage Based on Water-Soluble Organic Redox Couples,” *J. Electrochem. Soc.*, vol. 161, no. 9, Jun. 2014, doi: 10.1149/2.1001409jes.

[132] B. Huskinson *et al.*, “A metal-free organic–inorganic aqueous flow battery,” *Nature*, vol. 505, no. 7482, Jan. 2014, doi: 10.1038/nature12909.

[133] B. Huskinson, M. P. Marshak, M. R. Gerhardt, and M. J. Aziz, “Cycling of a Quinone-Bromide Flow Battery for Large-Scale Electrochemical Energy Storage,” *ECS Trans.*, vol. 61, no. 37, Sep. 2014, doi: 10.1149/06137.0027ecst.

[134] C. Wang *et al.*, “N-alkyl-carboxylate-functionalized anthraquinone for long-cycling aqueous redox flow batteries,” *Energy Storage Mater.*, vol. 36, pp. 417–426, Apr. 2021, doi: 10.1016/j.ensm.2021.01.019.

[135] M. T. Tsehaye *et al.*, “Study of Anion Exchange Membrane Properties Incorporating N-spirocyclic Quaternary Ammonium Cations and Aqueous Organic Redox Flow Battery Performance,” *Membranes*, vol. 11, no. 5, May 2021, doi: 10.3390/membranes11050367.

[136] T. Páez, A. Martínez-Cuezva, R. Marcilla, J. Palma, and E. Ventosa, “Mitigating capacity fading in aqueous organic redox flow batteries through a simple electrochemical charge balancing protocol,” *J. Power Sources*, vol. 512, Nov. 2021, doi: 10.1016/j.jpowsour.2021.230516.

[137] D. G. Kwabi, Y. Ji, and M. J. Aziz, “Electrolyte Lifetime in Aqueous Organic Redox Flow Batteries: A Critical Review,” *Chem. Rev.*, vol. 120, no. 14, Jul. 2020, doi: 10.1021/acs.chemrev.9b00599.

[138] H. Krämer and P. Meares, “Correlation of Electrical and Permeability Properties of Ion-Selective Membranes,” *Biophys. J.*, vol. 9, 1969.

[139] G. Pourcelly, “Conductivity and selectivity of ion exchange membranes: structure-correlations,” *Desalination*, vol. 147, no. 1, Sep. 2002, doi: 10.1016/S0011-9164(02)00609-4.

[140] Q. Dai *et al.*, “Thin-film composite membrane breaking the trade-off between conductivity and selectivity for a flow battery,” *Nat. Commun.*, vol. 11, no. 1, Jan. 2020, doi: 10.1038/s41467-019-13704-2.

[141] H. B. Park, J. Kamcev, L. M. Robeson, M. Elimelech, and B. D. Freeman, “Maximizing the right stuff: The trade-off between membrane permeability and selectivity,” *Science*, vol. 356, no. 6343, Jun. 2017, doi: 10.1126/science.aab0530.

[142] J. Li *et al.*, “Good practice guide for papers on batteries for the Journal of Power Sources,” *J. Power Sources*, vol. 452, Mar. 2020, doi: 10.1016/j.jpowsour.2020.227824.

[143] T. Liu, X. Wei, Z. Nie, V. Sprenkle, and W. Wang, “A Total Organic Aqueous Redox Flow Battery Employing a Low Cost and Sustainable Methyl Viologen Anolyte and 4-HO-TEMPO Catholyte,” *Adv. Energy Mater.*, vol. 6, no. 3, 2016, doi: 10.1002/aenm.201501449.

[144] B. Hu, C. DeBruler, Z. Rhodes, and T. L. Liu, “Long-Cycling Aqueous Organic Redox Flow Battery (AORFB) toward Sustainable and Safe Energy Storage,” *J. Am. Chem. Soc.*, vol. 139, no. 3, pp. 1207–1214, Jan. 2017, doi: 10.1021/jacs.6b10984.

[145] C. DeBruler *et al.*, “Designer Two-Electron Storage Viologen Anolyte Materials for Neutral Aqueous Organic Redox Flow Batteries,” *Chem*, vol. 3, no. 6, Dec. 2017, doi: 10.1016/j.chempr.2017.11.001.

[146] C. DeBruler, B. Hu, J. Moss, J. Luo, and T. L. Liu, “A Sulfonate-Functionalized Viologen Enabling Neutral Cation Exchange, Aqueous Organic Redox Flow Batteries toward Renewable Energy Storage,” *ACS Energy Lett.*, vol. 3, no. 3, Mar. 2018, doi: 10.1021/acsenergylett.7b01302.

[147] Y. Liu *et al.*, “A Long-Lifetime All-Organic Aqueous Flow Battery Utilizing TMAP-TEMPO Radical,” *Chem*, vol. 5, no. 7, pp. 1861–1870, Jul. 2019, doi: 10.1016/j.chempr.2019.04.021.

[148] C. Wang *et al.*, “High-Performance Alkaline Organic Redox Flow Batteries Based on 2-Hydroxy-3-carboxy-1,4-naphthoquinone,” *ACS Energy Lett.*, vol. 3, no. 10, Oct. 2018, doi: 10.1021/acsenergylett.8b01296.

[149] D.-R. Chang, Y. Kim, and S. Jung, “Comprehensive study of the performance of alkaline organic redox flow batteries as large-scale energy storage systems,” *Int. J. Energy Res.*, vol. 43, no. 9, 2019, doi: 10.1002/er.4573.
[150] K. Lin *et al.*, “Alkaline quinone flow battery,” *Science*, vol. 349, no. 6255, pp. 1529–1532, Sep. 2015, doi: 10.1126/science.aab3033.
[151] Z. Yang *et al.*, “Alkaline Benzoquinone Aqueous Flow Battery for Large-Scale Storage of Electrical Energy,” *Adv. Energy Mater.*, vol. 8, no. 8, p. 1702056, Mar. 2018, doi: 10.1002/aenm.201702056.
[152] P. Hu *et al.*, “Renewable-lawsone-based sustainable and high-voltage aqueous flow battery,” *Energy Storage Mater.*, vol. 19, pp. 62–68, May 2019, doi: 10.1016/j.ensm.2018.10.017.
[153] L. Tong *et al.*, “Molecular Engineering of an Alkaline Naphthoquinone Flow Battery,” *ACS Energy Lett.*, vol. 4, no. 8, pp. 1880–1887, Aug. 2019, doi: 10.1021/acsenergylett.9b01321.
[154] W. Lee, G. Park, and Y. Kwon, “Alkaline aqueous organic redox flow batteries of high energy and power densities using mixed naphthoquinone derivatives,” *Chem. Eng. J.*, vol. 386, p. 123985, Apr. 2020, doi: 10.1016/j.cej.2019.123985.
[155] C. Mirle, V. Medabalmi, and K. Ramanujam, “Crossover-free hydroxy-substituted quinone anolyte and potassium ferrocyanide catholyte for aqueous alkaline organic redox flow battery,” *Catal. Today*, vol. 370, pp. 173–180, Jun. 2021, doi: 10.1016/j.cattod.2020.12.012.
[156] H.-S. Choi, Y.-H. Oh, C.-H. Ryu, and G.-J. Hwang, “Characteristics of the all-vanadium redox flow battery using anion exchange membrane,” *J. Taiwan Inst. Chem. Eng.*, vol. 45, no. 6, Nov. 2014, doi: 10.1016/j.jtice.2014.08.032.
[157] J. Yuan *et al.*, “Membranes in non-aqueous redox flow battery: A review,” *J. Power Sources*, vol. 500, Jul. 2021, doi: 10.1016/j.jpowsour.2021.229983.
[158] B. Motealleh, Z. Liu, R. I. Masel, J. P. Sculley, Z. Richard Ni, and L. Meroueh, “Next-generation anion exchange membrane water electrolyzers operating for commercially relevant lifetimes,” *Int. J. Hydrog. Energy*, vol. 46, no. 5, Jan. 2021, doi: 10.1016/j.ijhydene.2020.10.244.
[159] X. Gao, H. Yu, F. Xie, J. Hao, and Z. Shao, “High performance cross-linked anion exchange membrane based on aryl-ether free polymer backbones for anion exchange membrane fuel cell application,” *Sustain. Energy Fuels*, vol. 4, no. 8, Jul. 2020, doi: 10.1039/D0SE00502A.
[160] S. Jeong, L.-H. Kim, Y. Kwon, and S. Kim, “Effect of nafion membrane thickness on performance of vanadium redox flow battery,” *Korean J. Chem. Eng.*, vol. 31, no. 11, Nov. 2014, doi: 10.1007/s11814-014-0157-5.
[161] H. Lee, M. Yanilmaz, O. Toprakci, K. Fu, and X. Zhang, “A review of recent developments in membrane separators for rechargeable lithium-ion batteries,” *Energy Environ. Sci.*, vol. 7, no. 12, Nov. 2014, doi: 10.1039/C4EE01432D.
[162] Y. Zhao, M. Li, Z. Yuan, X. Li, H. Zhang, and I. F. J. Vankelecom, “Advanced Charged Sponge-Like Membrane with Ultrahigh Stability and Selectivity for Vanadium Flow Batteries,” *Adv. Funct. Mater.*, vol. 26, no. 2, 2016, doi: 10.1002/adfm.201503390.
[163] M. T. Tsehaye *et al.*, “Pristine and Modified Porous Membranes for Zinc Slurry–Air Flow Battery,” *Molecules*, vol. 26, no. 13, Jan. 2021, doi: 10.3390/molecules26134062.
[164] M. Charyton, C. Iojoiu, P. Fischer, G. Henrion, M. Etienne, and M. L. Donten, “Composite Anion-Exchange Membrane Fabricated by UV Cross-Linking Vinyl Imidazolium Poly(Phenylene Oxide) with Polyacrylamides and Their Testing for Use in Redox Flow Batteries,” *Membranes*, vol. 11, no. 6, Jun. 2021, doi: 10.3390/membranes11060436.
[165] C. Ye *et al.*, “Development of efficient aqueous organic redox flow batteries using ion-sieving sulfonated polymer membranes,” *Nat. Commun.*, vol. 13, no. 1, Art. no. 1, Jun. 2022, doi: 10.1038/s41467-022-30943-y.
[166] A. Razmjou, M. Asadnia, E. Hosseini, A. Habibnejad Korayem, and V. Chen, “Design principles of ion selective nanostructured membranes for the extraction of lithium ions,” *Nat. Commun.*, vol. 10, no. 1, Dec. 2019, doi: 10.1038/s41467-019-13648-7.

[167] I. Salmeron-Sanchez, J. Asenjo-Pascual, J. R. Avilés-Moreno, J. C. Pérez-Flores, P. Mauleón, and P. Ocón, “Chemical physics insight of PPy-based modified ion exchange membranes: A fundamental approach,” *J. Membr. Sci.*, vol. 643, Mar. 2022, doi: 10.1016/j.memsci.2021.120020.

[168] H.-D. Nguyen *et al.*, “Nanostructured multi-block copolymer single-ion conductors for safer high-performance lithium batteries,” *Energy Environ. Sci.*, vol. 11, no. 11, 2018, doi: 10.1039/C8EE02093K.